DOI: https://doi.org/10.1016/j.quageo.2018.12.003

Radiometric dating of recent sediments: On the performance of ^{210}Pb-based CRS chronologies under varying rates of supply

J.M. Abril

Dpto. Física Aplicada I, ETSIA Universidad de Sevilla, Sevilla (Spain)
Carretera de Utrera km 1; D.P. 41013 Seville (Spain)
Email: jmabril@us.es; FAX: +34 954486436

Abstract

Radiometric dating was a revolutionary contribution to the study of sedimentary processes. Empirical data from varved sediments show that unsupported ^{210}Pb ($^{210}Pb_{exc}$) fluxes vary over time while they statistically correlate with sediment accumulation rates (SAR). This contradicts the basic assumption of the Constant Rate of Supply (CRS) model, which is the most widely used technique for recent sediments. This work is aimed at assessing the CRS model-errors by quantifying the effects on chronologies of various patterns of temporal variability of fluxes. Results are discussed through applications with synthetic and real cores for which and independent varve chronology or a set of reference dates are available. Periodic harmonic and random fluctuations in fluxes tend to cancel out positive and negative deviations in CRS ages, but they produce spurious variability in SARs. Persistent changes in fluxes lead to cumulated and unacceptable deviations of the CRS ages, which cannot be satisfactorily compensated by the use of a piecewise CRS model. The raw and piecewise CRS models can still be powerful tools of widespread use when the conditions for their applicability are well understood. The paper shows how the analysis of clusters in the $^{210}Pb_{exc}$ vs mass depth profile, along with the estimation of equivalent constant fluxes pre and post-dating a known reference date, are powerful methods to prevent misapplications of the CRS model.

Keywords: Radiometric dating; Recent sediments; CRS model; Varying fluxes; Model errors; Performance tests

1. Introduction

The radiometric dating of sediments is the only technique of general applicability that claims to provide an absolute age determination, and it has represented a revolutionary contribution to the study of the sedimentary processes (Carroll and Lerche, 2003). For recent sediments (< 100-150 y) the most common dating technique uses fallout ^{210}Pb, a natural radionuclide. The method was first proposed for dating glacier ice (Goldberg 1963) and it was first applied to lacustrine sediments by Krishnaswamy et al. (1971), and to marine sediments by Koide et al. (1972).

The primary object the researcher can handle after coring, sectioning and radiometric analysis, is the specific activity of ^{210}Pb found in excess ($^{210}Pb_{exc}$) with respect to its parent radionuclide (^{226}Ra) for each sediment slice, denoted hereafter as $A(m)$, with m being a mass-depth scale (mass depths are more meaningful than true depths because of natural compaction and the shortening during coring and storage). Although the physical fundamentals for the mass-conservation of a particle-bound radioactive tracer in porous and accreting sediments are relatively well understood (see the revisited diagenetic equations in Abril, 2003a), a $^{210}Pb_{exc}$ vs mass depth profile, by itself, is unable to provide any chronological information without the introduction of a series of assumptions. Any set of assumptions which enables the construction of a chronology from the above object is known as a radiometric dating model.

Most of the models share three assumptions: i) continuity of the sequence (i.e., there is not any missing layer by erosion, neither huge episodic depositional-events); ii) $^{210}Pb_{exc}$ behaves as a particle-associated tracer and new inputs are ideally deposited at the sediment-water interface (SWI) over the previously existing material; iii) there is not any post-depositional redistribution. Of course, they can be broken in particular sedimentary scenarios in the real world. Thus, mixing and diffusion have been widely reported and modelled (e.g., Robbins and Edgington, 1975; Christensen, 1982; Smith et al. 1986; Abril et al., 1992; Laissaoui et al. 2008). Non ideal deposition in sediments with high porosities in their upper sections has been described by Abril and Gharbi (2012). Erosive and/or depositional events have been described in some dynamic sedimentary systems (e.g., Arnaud et al., 2002; Abril et al., 2018). But, even when accomplished, the above assumptions are still unable to construct a chronology.

Figure 1 summarises the fundamental problem of a ^{210}Pb-based radiogeochronology. Given an $A(m)$ profile, one pursuits to extract a unique chronology, $T(m)$, which can be plotted as a continuous and monotonically increasing function in the age (T) versus mass depth (m) space. The sediment accumulation rate (SAR, with physical dimensions of $ML^{-2}T^{-1}$), denoted hereafter as w ($w = dm/dT$), is related with the local derivative of the chronological line:

$$\frac{dT}{dm} = \frac{1}{w} \quad (1)$$

Thus, any chronological line provides both age and SAR at any given mass depth, what enables decoding the $^{210}Pb_{exc}$ profile to reconstruct the history of initial activity concentrations and the palaeofluxes onto the SWI. One can use the so obtained time series of fluxes and SARs as inputs for solving the mass-conservation equation for a radioactive tracer in sediments (Abril, 2003a); and the solution will be exactly the given $A(m)$. Obviously, without any additional restrictive assumption, there are an infinite number of possible chronological lines being all of them mathematically exact solutions (see Fig.1, panel 1, and a more detailed discussion in Abril, 2015).

Examples of additional assumptions enabling unique solutions are: i) $^{210}Pb_{exc}$ fluxes onto the SWI are constant over time (CRS model; Appleby and Oldfield, 1978); ii) initial activity concentrations are constant over time (CIC model; Goldberg, 1963); iii) fluxes onto the SWI and SAR are both constant over time (CF-CS model; Robbins, 1978) ; iv) fluxes and SARs can independently vary over time, but imposing a particular (and non-physically justified) choice for a Fourier series expansion (SIT model; Carroll and Lerche, 2003; Abril, 2015); v) varying $^{10}Pb_{exc}$ fluxes and SARs, but attaining a positive statistical correlation, as shown by Abril and Brunskill (2014) (TERESA model; Abril, 2016). It is worth noting that the above unique solutions become a restricted set of solutions when accounting for the analytical and propagated uncertainties.

At a best, the accomplishment of these restrictive assumptions will be only approximate. Consequently the model chronology may show positive and negative (but overall compensated) deviations from the true chronology and thus, being reasonably acceptable (Fig.1, panel 2). Nevertheless, local derivatives may be much affected, leading to spurious local high or low SAR values which do not correspond to any environmental change. In consequence, an acceptable model-chronology does not necessarily imply a high-resolution high-accurate SAR history.

Each one of the above five model-assumptions represents a paradigm on the behaviour of $^{210}Pb_{exc}$ fluxes onto the SWI in aquatic sedimentary systems. But, what does the direct empirical evidence say about that? The deposition rate of atmospheric ^{210}Pb is influenced largely by rainfall, leading to large annual variations (30–50 %) in measured $^{210}Pb_{exc}$ deposition (Turekian et al., 1977; Rangarajan et al., 1986). Inter-annual variations more than two-fold have also been reported (Winkler and Rosner, 2000). After atmospheric deposition, ^{210}Pb can follow a wide diversity of pathways to reach the SWI. These $^{210}Pb_{exc}$ fluxes onto the SWI are the meaningful ones for radiometric dating.

Varved sediments allow for establishing a complete and independent chronology, enabling the reconstruction of records of $^{210}Pb_{exc}$ palaeofluxes, initial activity concentrations, and SARs (Abril and Brunskill, 2014). This provides a unique chance for getting direct empirical evidences on the behaviour of $^{210}Pb_{exc}$ fluxes. Based upon a wide and systematic survey on laminated sediments from marine, riverine and lacustrine environments, Abril and Brunskill (2014) found that $^{210}Pb_{exc}$ fluxes onto the SWI were governed primarily by fluxes of matter, rather than by direct atmospheric deposition, being highly variable in time and statistically correlated with SAR(see a summary of the statistical analysis in Fig. ESM-1, in electronic supplementary material). This result can be well understood from composite mass-flows carrying $^{210}Pb_{exc}$ inputs, both with intrinsic scatter (Abril and Brunskill, 2014). The range of variability in weather conditions leads to varying intensities in the flows of mass and $^{210}Pb_{exc}$ from the scavenging processes and from all the potential erosional areas contributing to the final fluxes onto the SWI at the studied site. These findings provide a new paradigm for interpreting $^{210}Pb_{exc}$ fluxes onto the SWI, which replaces the old view of fluxes dominated by direct atmospheric deposition (Binford et al., 1993).

At this point all the classical models need to be revisited under the light of this empirical evidence. TERESA model (Abril, 2016) was developed just using this new paradigm. Its applications till present are scarce (Abril, 2016; Botwe et al. 2017; Klubi et al., 2017) and more experience is needed to better explore the potentials and limitations of this model. The SIT model claims its ability for stablishing chronologies with fluxes and SARs independently varying over time, and it contains the new paradigm as a particular case. Nevertheless, it has been shown that this model lacks of a sound physical basis and, in particular, it makes a misuse of the Fourier series expansions (Abril, 2015).

The CRS model is the most widely used ^{210}Pb-based radiometric dating model for recent sediments; it contains the CF-CS model as a particular case, and thus it is the focus of the present study.

The new paradigm on fluxes seems to contradict the basic CRS model assumption of a constant rate of supply. But in many application cases the CRS model has been validated against independent chronostratigraphic markers (e.g. ^{137}Cs and ^{241}Am peaks). How conciliate these contradictory results? What level of support actually provides a single independent date? Particularly, when varve dates are available, allowing testing the CRS-ages over the whole range of the chronology, the CRS model has shown good performance in some cases (e.g., Appleby et al., 1979; Lima et al. 2005; Shanahan et al., 2008), while it failed in others (e.g., Wan et al., 1987; Reinikainen et al., 1997; Lamoureux, 1998; Finsinger et al., 2006; Chutko and Lamoureux; 2009; Tylmann et al., 2013).

With time, the viewpoint of researchers has evolved regarding the role of $^{210}Pb_{exc}$ fluxes onto the SWI when applying the CRS model. Initially it was dominated by the view of a constant atmospheric deposition. Thus, the criteria for the reliability of the CRS assumptions included that the measured inventory should be within a range expected from regional atmospheric fallout rate, and that multiple cores within a lake, but from areas of different sediment accumulation rates, should have similar $^{210}Pb_{exc}$ inventories (Binford et al., 1993). As the contribution of the $^{210}Pb_{exc}$ associated to mass flows from the catchment and other sedimentary areas became clearer, it resulted evident that the application of CRS was still possible with fluxes of a composite nature and origin, while they remained constant over time (e.g. Oldfield et al., 1995). This paper will extend this view by proving that the raw CRS chronologies can be acceptable even for varying rates of supply positively correlated with SAR, when such variations are randomly sorted in time around a mean value. This is, the new paradigm always has been there, but in a large number of study cases it has been (it is) compatible with CRS chronologies.

The idea that the mean value of $^{210}Pb_{exc}$ fluxes onto the SWI can undergo important drifts over time is not new. Indeed, this result is evident in many cases where the ^{137}Cs time-marks (or other chronostratigraphic marks) allow estimating the equivalent constant fluxes from the partial $^{210}Pb_{exc}$ inventories lying within two consecutive reference dates (see the methodology in Appleby, 2001). The piecewise CRS model (Appleby, 2001) has been proposed as a suitable radiogeochronological tool for cases where the fluxes pre and post-dating a known reference date are significantly different. This is illustrated in Fig. 2 (panel 1), where both the raw and the piecewise CRS models are applied to a $^{10}Pb_{exc}$ vs mass depth profile for which two ^{137}Cs time-marks are known (the Chernobyl accident and the 1963 peak in bomb-derived fallout, respectively; data from Tylmann et al., 2016). The piecewise CRS has been applied twice: i) using only the 1963 reference date; ii) using both ^{137}Cs time marks. In the first case two periods or transects of different constant $^{210}Pb_{exc}$ fluxes have been defined from the above time marks and partial inventories, namely (in the order of increasing ages): 396 ± 8, and 692 ± 28 $Bq{\cdot}m^{-2}\ y^{-1}$. In the second application the first transect is divided into two new transects by the Chernobyl reference date, with fluxes of 319 ± 8 and 568 ± 18 $Bq{\cdot}m^{-2}\ y^{-1}$, respectively.

As seen in Fig. 2, it is evident that chronologies depend on the number of the included reference dates. Indeed, transects are defined by the reference dates, not because this was physically reliable but just because it is mathematically feasible. It is certain that the true ages and the piecewise CRS ages agree at the reference points (and at the surface), but this is not an outcome of the model, but just an imposed condition for its construction. It is worth noting that this imposed agreement is quite often interpreted as the endpoint in the dating of the sediment core, without paying any more attention to the effects of model-errors (those arising from a partial or null accomplishment of the model assumptions). There may be two major sources of model-errors in a piecewise CRS model: i) the flux onto the SWI follows an stepped function, as assumed in the model, but the true age of the discontinuity falls far from the reference date used in the model; ii) the flux onto the SWI does not follows a stepped function but it undergoes continuous trends of change.

It is assumed that the piecewise CRS-chronology provides a proxy to the true one, but in most of the cases there are no means to known how good such a proxy is. In this example there is an independent chronology from varves (Tylmann et al., 2016). Figure 2, second panel, shows the deviations of the piecewise CRS chronologies with respect the one from varves. Discrepancies are relevant. In the figure error bars account for the analytical and propagated uncertainties, which could be minimized by improved instrumental methods, but the systematic deviations obey to model-errors (this case will be further considered in this paper, including the reconstruction of records of palaeofluxes).

A strong conservative criterion would reject the chronology for any transect not ending in a well-defined independent reference date. But this does not warrant the accuracy of the CRS ages, as seen for the first transect in both piecewise applications. A more dense set of reference dates would certainly improve the accuracy of the piecewise CRS ages, but this could be hardly achievable in most of the studied sites, and, when possible, the ^{210}Pb-based chronology would be rather redundant, since the one based on simple linear interpolations or smooth fits to the reference dates could be then suitable enough (as illustrated in Fig.2, panel 2).

For different reasons, independent chronostratigraphic marks are not always available, or they may be not confident enough (Abril 2003b; 2004). In practice, a huge number of scientific works involving the radiometric dating of recent sediments continue being published only with $^{210}Pb_{exc}$ data. This justify the interest in developing strategies for identifying some patterns of varying rates of supply from the analysis of the $^{210}Pb_{exc}$ vs mass depth profiles. As demonstrated in the paper, this is possible in some cases by using the new paradigm on fluxes by Abril and Brunskill (2014).

All the above issues demand a better understanding of the model-errors in the CRS-based chronologies, being this the aim of the present work. We try to understand and quantify the effects on CRS chronologies of various patterns of temporal variability of fluxes (e.g., random variability versus persistent changes) and to elucidate which of them, if any, can be compensated with a piecewise CRS model. The paper will also propose some mathematical tests for the reliability of a CRS-chronology based upon the analysis of the $A(m)$ dataset, and it will suggest some practical guidance for avoiding misuses of the CRS model.

2. Materials and Methods

2.1. *The CRS model*

A detailed model formulation can be seen in Appleby and Oldfield (1978), or in Sánchez-Cabeza and Ruíz-Fernández (2012). In brief, the model assumes that $^{210}Pb_{exc}$ fluxes onto the SWI, F, are constant over time. The $^{210}Pb_{exc}$ inventory below the sediment horizon at mass depth m, Σ_m, is:

$$\Sigma_m = \int_m^{\infty} A(m')dm' \qquad (2)$$

In practice, the integral is replaced by a discrete summation over all the sediment slices below mass depth m. The total inventory below the SWI, Σ_0, is given by Eq. 2 for $m = 0$. When fluxes have remained constant over periods of time larger than several ^{210}Pb half-lives, Σ_0 reaches a steady state (i.e. the flux at the SWI compensates for the radioactive decay of Σ_0): $F = \lambda\, \Sigma_0$, with λ being the radioactive decay constant for ^{210}Pb. The sediment horizon when at the time of sampling is at mass depth m, was the former SWI at age t_m. The condition of steady state inventory implies that $\Sigma_m = \Sigma_0 e^{-\lambda t_m}$, what allows solving the chronology:

$$t_m = \frac{1}{\lambda}\ln\left(\frac{\Sigma_0}{\Sigma_m}\right) \tag{3}$$

The SAR history can be then solved from Eq. 1 (in practice derivatives are approached by finite differences of mass-depths and ages), what may involve large propagated uncertainties. Alternatively, the value of SAR at age t_m, w_m, can be estimated by imposing the condition that the advective flux through the sediment horizon at mass depth m, $w_m A(m)$, compensates for the radioactive decay of Σ_m (Appleby and Oldfield, 1978):

$$w_m = \lambda\frac{\Sigma_m}{A(m)} \tag{4}$$

This procedure involves smaller propagates uncertainties, but it introduces a new assumption which is not really needed for the CRS model; namely that any Σ_m remains steady-state, what implies that $A(m)$ is also steady-state.

A detailed study on the involved analytical and propagated uncertainties in the CRS model can be found in the works by Binford (1990) and MacKenzie et al. (2011). This last work shows that the CRS ages (Eq. 3) are quite sensitive to an accurate estimation of Σ_0. Nevertheless, the present work is concerned with model-errors, i.e., those arising from a partial or null accomplishment of the model assumptions.

The work by Appleby (1998) provides a review of the CRS model, its problems and solutions. The associated techniques for using a piecewise CRS model can be found in the above work, and in Appleby (2001). They will be briefly presented some further, when needed.

2.2. *Assessment of model errors in a CRS-chronology*

Abril and Brunskill (2014) provided an estimate of the error in the CRS ages and SARs due to a varying rate of supply. It is not general enough, but quite intuitive for a first level of analysis. If Σ_0 is the $^{210}Pb_{exc}$ inventory below the SWI in a sediment core at time t = 0, the ''equivalent constant flux'' is defined as $F_e = \lambda\, \Sigma_0$. During the next elapsed time Δt, a new flux, F, which may be different from F_e but assumed to be constant during this time interval, enters the SWI. The new total inventory, Σ_0^*, and the inventory below the former SWI, Σ_b^*, are, respectively:

$$\Sigma_0^* = \frac{F}{\lambda}\left(1 - e^{-\lambda\Delta t}\right) + \Sigma_b^* \quad ; \Sigma_b^* = \Sigma_0\, e^{-\lambda\Delta t}.$$

With both inventories, the CRS model estimates the elapsed time

$$\Delta t_{CRS} = \frac{1}{\lambda}\ln\left(\frac{\Sigma_0^*}{\Sigma_b^*}\right)$$

The absolute deviations in chronology, $\delta_T = \Delta t_{CRS} - \Delta t$, can be estimated with a first-order expansion of the exponentials (Abril and Brunskill, 2014):

$$\delta_T = (k - 1)\Delta t; \tag{5}$$

where $k = F/F_e$. The deviation in chronology can be positive or negative, for F higher or lower than F_e, respectively. This expression provides a first intuitive insight. If we iterate the process for subsequent time intervals, the cumulative deviation in the chronology may result negligible when positive and negative deviations cancel out among them. This is expected to happen when changes in F are randomly distributed in time around its mean value. On the contrary, if a trend of increasing/decreasing in fluxes is maintained for a large period of time, then deviations in chronology are of the same sign and they accumulate leading to a significant deviation from the true chronology.

In the above approach, the value of F_e must be updated with each iteration, what introduces additional mathematical complexity. A more comprehensive approach can be achieved by adopting a time (age) scale in which the origin is fixed at the time of sampling of the sediment core. The flux onto the SWI at age t before sampling can be written as a baseline value, F_0, plus a deviation from such reference: $F(t) = F_0 + \delta_F(t)$. It is worth noting that F_0 does not need to be coincident with F_e nor with the arithmetic mean of $F(t)$. The total inventory and the inventory below the sediment horizon at mass depth m (with age t_m), are:

$$\Sigma_o = \int_0^\infty [F_0 + \delta_F(t)]e^{-\lambda t}dt \ , \Sigma_m = \int_{t_m}^\infty [F_0 + \delta_F(t)]e^{-\lambda t}dt, \tag{6}$$

respectively. The CRS age for the sediment horizon at mass depth m, $t_{CRS}(t_m)$ is then given by Eq. 3, and the deviation with respect to the true chronology, $\delta_T(t_m) = t_{CRS} - t_m$.

Equations 6 and 3 can be numerically solved for any stated $F(t)$. Analytical solutions will be provided for fluxes onto the SWI with periodic-harmonic fluctuations around the baseline value; for fluxes with random variations, also randomly distributed in time; for stepped changes in fluxes and for linear trends of increase/decrease. The factors controlling the magnitude of absolute deviations with respect to the true chronology will be studied. This will provide a suitable basis for understanding the limits on the performance of the raw and the piecewise CRS models.

2.3. *Mathematical tests for the assessment of the performance of a CRS-chronology*

In electronic supplementary material it will be proved the following theorem: In absence of restrictive assumptions on the variability of fluxes and SARs (the paradigm of the SIT model), any Σ_m versus t_m profile can be translated into an infinite number of different $A(m)$ profiles. Inversely, any $A(m)$ profile, without restrictive assumptions else than ideal deposition, continuity of the sequence, and non postdepositional redistribution, can be associated to an infinite number of $\Sigma_m(t_m)$ profiles.

The above result invalidates any attempt for identifying fingerprints (or for developing mathematical tests) in $A(m)$ (the primary object for the radiogeochronology) to evaluate *a priori* the performance of the CRS model.

Nevertheless, $^{210}Pb_{exc}$ are statistically correlated with SARs (Abril and Brunskill, 2014). As shown in Fig. ESM-1, this correlation arises from the combination of a random and independent variability in the initial activity concentrations, A_0, and SARs, w, around their respective arithmetic mean values (estimated for the whole record):

$$A_0 = \langle A_0 \rangle + \delta_A \quad ; \quad w = \langle w \rangle + \delta_w \quad ; \quad F = A_0 w \qquad (7)$$

In the above expression < > denotes the arithmetic mean, and δ_A, δ_w are the random deviations in the values of the initial activity and SAR, respectively. In practice, a couple of values (A_0, w) can be ascribed to each sediment slice sectioned for radiometric analysis. As variabilities in A_0 and SARs are independent (Fig. ESM-1),

$$\langle F \rangle = \langle A_0 \rangle \langle w \rangle \qquad (8)$$

The new TERESA model (Abril, 2016) is based upon this statistical correlation, and it is able to solve time arrangements of initial activity concentrations and SARs which are not randomly sorted in time.

When randomly distributed in time, the effect of such variability in A_0 and SAR when applying the CIC model is that the CIC-ages fluctuate around the trend-line which provides the meaningful chronology. Also in these cases the CF-CS model can show good performance. When persistent changes in environmental conditions shift the initial concentrations and/or the SARs towards different mean values, the plot Ln[$A(m)$] can show jump discontinuities and/or changes in the slope. Examples of real cases where these changes happen will be presented and discussed in subsection 3.6. But not all the observed discontinuities can be linked to situations with changes in <*F*>. To distinguish such changes, <A_0>, <*w*> and <*F*> can be estimated from the plot by using a piecewise CF-CS model.

Figure 3 shows an sketch for a Ln[$A(m)$] plot with two discontinuities and three transects which are separately fitted to straight lines, providing (negative) slopes s_i and ordinates in origin *bi*. For the first transect (for simplicity the notation < > is omitted for the mean values):

$$A_{0,1} = e^{b_1} \quad ; \quad w_1 = \frac{\lambda}{s_1} \quad ; \; F_1 = A_{0,1} w_1 \tag{9}$$

For the second transect, with different mean values for initial activity and SAR, the fitting parameters must be estimated for the function

$$A(m') = A_{0,2} \exp\left[-\lambda\left(\frac{m_1}{w_1} + \frac{m'}{w_2}\right)\right];$$

with $m'=m-m_1$; thus,

$$b_2 = \mathrm{Ln}\left(A_{0,2}\right) - m_1 s_1 \; ; \; w_2 = \lambda/s_2. \tag{10}$$

For the third transect the fitting parameters correspond to the function

$$A(m') = A_{0,3} \exp\left[-\lambda\left(\frac{m_1}{w_1} + \frac{m_2 - m_1}{w_2} + \frac{m'}{w_3}\right)\right];$$

with $m'=m-m_2$, and

$$b_3 = \ln\left(A_{0,3}\right) - s_1 m_1 - s_2(m_2 - m_1) \; ; \; w_3 = \lambda/s_3. \tag{11}$$

It is worth noting that the effect of using m' is a uniform translation of the origin of coordinates, what minimizes the fitting uncertainties in b_2 and b_3. These approaches will provide a basis for studying real cases of $^{210}Pb_{exc}$ profiles and for identifying those situations in which the CRS model can fail (subsections 3.5 and 3.6).

2.4. Core data

For testing the performance of the CRS model, this work uses sediment core data from published scientific works (references are provided in each particular case) for which a varve chronology and/or a set of reference dates are available. Reconstructions of palaeofluxes onto the SWI are reported in some cases following the methodology described in Abril and Brunskill (2014). Synthetic cores are also used in this work. They have been generated following the methodology described in Abril (2016), which involves realistic bulk density profiles and a random and independent variability in SAR and initial activity concentrations around their respective mean values, over which different trends of change are imposed.

The statistical software package Statgraphics Centurion XVI has been used for linear regression analysis and for the estimation of the Durbin-Watson statistic.

3. Results

3.1. *Fluxes onto the SWI with periodic-harmonic fluctuations around the baseline value.*

For a harmonic fluctuation of amplitude B and period T_p, the fluxes onto the SWI can be mathematically written as:

$$F(t) = F_0 + Bcos(\frac{2\pi}{T_p}t + \varphi) \quad , \tag{12}$$

where φ describes the state of the fluctuation at the time of sampling (t=0). The analytical solution of Eq. 6 for Σ_m is (it is relatively straightforward when working in the space of complex numbers):

$$\Sigma_m = \frac{F_0}{\lambda}e^{-\lambda t_m} + \frac{Be^{-\lambda t_m}}{\lambda^2 + (\frac{2\pi}{T_p})^2}\left[\lambda\cos\left(\frac{2\pi}{T_p}t_m + \varphi\right) - \frac{2\pi}{T_p}\sin\left(\frac{2\pi}{T_p}t_m + \varphi\right)\right] \tag{13}$$

For $t_m = 0$ we get the expression for Σ_o; and then we can solve for the CRS chronology (Eq. 3) and $\delta_T(t_m)$, the deviations from the true chronology, as a function of the age t_m. It is worth noting that for B=0 Eq.13 gives the solution for a constant rate of supply.

As an example, Fig. 4 plots the solutions for $\delta_T(t_m)$ corresponding to a baseline of $F_0 = 100$ Bq·m^{-2}·y^{-1}, and various values for B, T_p and φ. Deviations from the true chronology show oscillations with the same period T_p, with amplitudes being proportional to the amplitude of the oscillations in fluxes, B, and they growth with T_p. For φ=0 or φ=π, the flux is at its maximum or its minimum value at the time of sampling (Eq. 12), and the oscillations in δ_T are centred on the true chronology (Fig. 4). For φ=π/2 and φ=3π/2, the flux is at is baseline level, and the oscillations in δ_T are systematically displaced down or up of the true chronology, what maximizes the absolute deviation (Fig. 4).

For $T_p < 20$ y, the angular frequency of the oscillation is one order of magnitude higher than λ, what allows simplifying Eq. 13, and, in a first order expansion, one can find that (for φ=π/2 and φ=3π/2)

$$\delta_{T,\,max} \sim 10\lambda T_p B/F_0. \tag{14}$$

3.2. *Fluxes onto the SWI with random variability.*

Although not properly periodic, random oscillations around the baseline value for fluxes, when also randomly sorted in time, depict a situation close to the above problem. Thus, one can expect that the CRS ages will also compensate positive and negative deviations with respect to the true chronology. This can be tested with the synthetic core of Fig. 5, generated following the methodology described by Abril (2016). It involved a realistic bulk density profile and normal distributions for initial activity and SARs with mean values of 250 $Bq\cdot kg^{-1}$ and 0.18 $g\cdot cm^{-2}y^{-1}$, and standardized deviations of 0.2 and 0.25, respectively. This leads to fluxes onto the SWI with random variations and randomly distributed in time (Fig. 5), and to the $^{210}Pb_{exc}$ vs mass depth profile shown in Fig.5. Application of the raw CRS model involved the usual correction for the total inventory based upon the extrapolation of the exponential trend prevailing at the deepest portion of the core. The so obtained CRS ages reasonably fit the true chronology (this last arises from the values of SAR and mass thickness for each sediment slice), as shown in Fig.5. Finally, a comparison among CRS and true SARs is also depicted in Fig. 5 (error estimates have been omitted - see above comments in the Introduction section). The order of magnitude and the global trends are well reproduced, but a high resolution and high accurate SAR history cannot be expected from any of the existing radiometric dating models.

3.3. *Fluxes onto the SWI with stepped variations and continuous trends of increase/decrease.*

The stepped $F(t)$ function shown in Fig. 6a will provide a framework general enough for the present goals. The value of Σ_m (Eq. 6) can be analytically solved for the three regions of ages:

a) $t_m > t_2$

$$\Sigma_m = \frac{F_0}{\lambda} e^{-\lambda t_m}$$

b) $t_1 < t_m < t_2$

$$\Sigma_m = \frac{F_0}{\lambda} e^{-\lambda t_m} + \frac{B}{\lambda}\left(e^{-\lambda t_m} - e^{-\lambda t_2}\right) \qquad (15)$$

c) $t_m < t_1$

$$\Sigma_m = \frac{F_0}{\lambda} e^{-\lambda t_m} + \frac{B}{\lambda}\left(e^{-\lambda t_1} - e^{-\lambda t_2}\right)$$

The value of Σ_0 follows from the last expression for $t_m = 0$, what allows estimating CRS ages after Eq. 3, and then $\delta_T(t_m)$.

Figure 7 plots some results for a baseline of $F_0 = 100$ Bq·m^{-2}y^{-1} and for various values of B, t_1 and $DT = t_2 - t_1$. When t_1 >0 there are three transects in Fig. 6a, and the CRS model seems to interpret them as positive and negative deviations around a mean value. This leads to positive and negative deviations in the chronology with a relatively low maximum absolute-deviation (this value, for equal *DT,* increases as more recent is the stepped changed, as shown in Fig. 7). For t_1=0 the situation corresponds to two periods of time with distinct but constant flows onto the SWI. In this case δ_T growths from zero at the SWI (i.e., t =0) till reaching its maximum value, which remains then constant downcore (Fig. 7). The value of $\delta_{T,max}$ increases with the B/F_0 ratio and with the duration of the change, $DT = t_2$. An analytical expression for $\delta_{T,max}$ can be obtained from Eqs. 15a and 15b when t_1=0:

$$\delta_{T,max} = \frac{1}{\lambda} \ln\left[1 + \frac{B}{F_0}\left(1 - e^{-\lambda t_2}\right)\right] \qquad (16)$$

Thus, the CRS chronologies can result unacceptable in this situation; e.g., a $\delta_{T,max}$ $= 10$ y can be achieved for B/F_0 = 0.8 with t_2=19.5 y, B/F_0 = 0.5 with t_2=42 y or B/F_0 = 0.4 with t_2=80 y.

In Fig. ESM-2 (in electronic supplementary material) this study is extended to situations in which fluxes onto the SWI continuously increase/decrease at a constant rate in recent years ($t < t_1$), as shown in the sketch of Fig. 6b. The deviations in the CRS ages increase with both, the cumulated change in fluxes and the duration (Fig. ESM-2), and they can surpass 10 years in a wide range of realistic situations (e.g., when fluxes increase up to doubling their initial value during the last 32 years).

3.4. *Performance of the piecewise CRS model for F(t) with stepped variations*

In this subsection we explore the capability of the CRS model to overcome the situations described in the previous subsection 3.3 when a reference date is known (usually the ^{137}Cs and/or the $^{239+240}$Pu peaks in their profiles in the sediment core, associated to the dates of their maximum atmospheric deposition).

A piecewise CRS model assumes that the whole temporal range of the chronology can be divided into two or more periods or transects with constant $^{210}Pb_{exc}$ fluxes, although with different values for each period. Transects are defined by the reference dates. When only a reference date is available, t_r, the first constant flux for the interval $[0, t_r]$, $F_{pw,1}$, can be estimated from the measured partial inventory comprised from the SWI to the sediment horizon at mass depth m_r whose age t_r is known, $\Sigma(0,m_r) = \Sigma_0 - \Sigma_{m_r}$:

$$\Sigma(0,m_r) = \int_0^{t_r} F_{pw,1} e^{-\lambda t} dt \qquad (17)$$

The flux $F_{pw,2}$, for the second transect (t_r, ∞), can be estimated from the inventory below m_r:

$$\Sigma(m_r,\infty) \equiv \Sigma_{m_r} = \int_{t_r}^{\infty} F_{pw,2} e^{-\lambda t} dt \qquad (18)$$

The piecewise CRS age of a sediment horizon at mass depth m, of true age t in the interval $[0, t_r]$, can be estimated as

$$t_{CRS} = \frac{1}{\lambda} ln\left[\frac{F_{pw,1}}{F_{pw,1} - \lambda\, \Sigma(0,m)}\right], \qquad (19)$$

where $\Sigma(0,m) = \Sigma_0 - \Sigma_m$. Similarly, the piecewise CRS age of a sediment horizon of true age t in the interval (t_r, ∞) –i.e. with $m > m_r$, is:

$$t_{CRS} = t_r + \frac{1}{\lambda} ln\left[\frac{\Sigma_{m_r}}{\Sigma_m}\right]. \qquad (20)$$

Figure 8 shows results for three examples of stepped fluxes described by Fig. 6a. Panel a) in Fig. 8 shows the case of an ideal stepped flux with three transects (with discontinuities at ages 15 and 70 y) which is intended to be modelled by a piecewise

CRS model using a single reference date. It is worth noting that in practice the true flux history is unknown for the researcher, and a piecewise model with a reference date can be a routinely approach. The model exercise has been replicated for three different values of the reference date, namely 30, 50 and 65 y, which produce pairs of “constant equivalent fluxes” post and pre-dating the reference date of (138.6, 171.2), (152.7, 146.3) and (157.0, 114.4), respectively (values in $Bq \cdot m^{-2} y^{-1}$). As shown in Fig. 8a, deviations of the CRS-chronologies are quite noticeable in all the cases, although smaller for the reference date of 65 y, close to one of the true discontinuities. It is worth noting that the second reference date, of 50 y, leads to estimates of equivalent constant fluxes which are similar for the two transects, what could be routinely interpreted as a reasonable proof for constant fluxes, supporting then the application of the raw CRS model (also depicted in Fig. 8a for the sake of comparison). Finally, Fig. 8a also shows that a piecewise CRS model does not necessarily provide a better estimate of ages than a raw CRS model.

Panel b) in Fig. 8 shows the case of an ideal stepped flux with two transects (with discontinuity at age 45 y) which is intended to be modelled by a piecewise CRS model. By using the above three different reference dates of 30, 50 and 65 y, the corresponding pairs of “constant equivalent fluxes” post and pre-dating the reference date are of (170.0, 126.1) , (166.8, 100.0) and (160.8, 100.0), respectively (values in $Bq \cdot m^{-2} y^{-1}$). In this case all the tests based upon the reference dates indicate noticeable long-term variations in fluxes. In this example, the piecewise CRS model provides a better proxy to the true ages than a raw CRS model. Again the best estimate is achieved for a reference date (50 y) close to the age of the true discontinuity (45 y).

Panel c) in Fig. 8 depicts a situation similar to that of Fig. 8b, but with fluxes decreasing in recent years. Again, the best proxy to true ages is achieved when the reference date is close to the age of the true discontinuity.

An example of a piecewise CRS model with two reference dates has been presented in Fig. 2, involving a real case-study, and it will be further discussed in subsection 3.6. The methodology for using a piecewise CRS model with several reference dates can be seen in the work by Appleby (2001).

3.5. *On the existence of fingerprints or statistical tests for an a priori evaluation of the performance of the CRS model.*

Under the paradigm of fluxes and SARs independently varying over time (the one of the SIT model), there are no means for unambiguously identifying any fingerprint of varying fluxes in the $A(m)$ profile (see demonstration in Appendix ESM-A, in electronic supplementary material). But Abril and Brunskill (2014) have shown that a positive statistical correlation between them seems to hold in most of the cases (see details in the above reference, in the Methods section and in Fig. ESM-1). This allows tracking those changes in fluxes that may result in unacceptable CRS chronologies. Table 1 summarises the effects of some temporal changes (in the sense of increasing ages and m) of A_o, and SAR in the Ln[$A(m)$] plot, and their implications for ^{210}Pb fluxes onto the SWI and for the applicability of the CRS model. Examples with practical applications follow in the next subsection. On the basis of those examples the performance of the Durbin-Watson statistic will be also studied (subsection 3.7).

3.6. *Applications to synthetic and real-case sediment cores from literature data*

Core V1: Varved sediment from Pettaquamscutt River basin

Data from Lima et al. (2005). Sediment core from Pettaquamscutt River basin (Rhode Island, Northeast USA), sampled on April 1999 at 41º30'N, 71º26'W and 19.5 m of water depth. The core showed varves with biogenic and clastic layers. Abril and Brunskill (2014) reconstructed the palaeofluxes and SAR history for this core; the former are shown in Fig. 9. They show large variability randomly distributed around their mean value. It is worth noting that palaeofluxes are not generally available, and the researcher must build the chronology only from the primary object $A(m)$.

Figure 9 shows the Ln[$A(m)$] plot for this core, with a jump discontinuity and a change in the slope. The fitting parameters for a piecewise CF-CS model appear in Table 2. In the sense of increasing ages and m, the initial activity shifts up to twice its previous value, while SAR decreases by a factor about 2. This keeps the mean value for fluxes virtually constant (Table 2), as in the case e) of Table 1. The (mean) values of the fluxes obtained from the piecewise CF-CS model (Table 2) compare well with the reconstructed palaeofluxes (Fig. 9). In absence of the varve chronology, and taking into account the involved uncertainties in the estimation of parameters (Table 2), there are no means for discarding the application of the CRS model to this core.

The application of the raw CRS model (Fig. 9, second panel) shows a good performance for most of the range of the chronology when compared against the ages estimated from varves. Nevertheless, the CRS model overestimated ages in the deepest portion of the core, although with large involved uncertainties.

In this case, the origin of discrepancies cannot be resolved from the usual difficulties found in dating sediment layers older than a century without high-resolution and accurate data (MacKenzie et al., 2011). It is worth noting that corrections for the total inventory were applied, as usual, by accounting for the extrapolated exponential trend of $A(m)$ in the deepest section of the core. This correction account for less than 0.6% of the total inventory, but it has a major effect in the older CRS ages. Thus, a correction of 1.8% for the total inventory allows fitting the CRS and varve ages (not shown).

Lima et al. (2005) also reported data on ^{137}Cs, whose 1963 time-mark was comprised in the region of good performance of the CRS model (m= 2.28 g·cm^{-2}). Furthermore, this reference date allows estimating post and pre-dating constant equivalent fluxes of 335 ±19 and 303±8 Bq·m^{-2}y^{-1}, respectively, without statistically significant differences at 95% confidence level.

Core V2: Varved sediment from Sihailongwan Lake

Data from Schettler et al. (2006a). Sediment core from Sihailongwan Lake (Northeast China, Jilin Province), sampled on September 1999 at 42º17'N, 126º36'W and at 50 m water depth. The core showed varves with biogenic and clastic layers. Reconstructed palaeofluxes for this core were provided by Schettler et al. (2006a), and revisited by Abril and Brunskill (2014). They are shown in Fig. 10 (first panel). Fluxes fluctuated within the range 330-660 Bq·m^{-2}y^{-1} except for the uppermost sediment layers, with lower values, around 250 Bq·m^{-2}y^{-1}.

For this study the $A(m)$ profile has been truncated by omitting data from slice number 5, since it registered episodic high deposition likely linked to a dust storm event (Schettler et al. 2006b).Truncation has been applied as in Arnaud et al., 2002. Also in this case the correction to the total inventory was negligible (< 0.1%). It is worth noting that authors provided ^{210}Pb without their associated uncertainties, but measurements were carried out by alpha spectrometry, and relative uncertainties of 5% have been assumed for the present estimations, following the same criteria than in Abril and Brunskill (2014), in their study of this core.

The Ln[$A(m)$] plot for this core (Fig. 10) shows a jump discontinuity with change in the slope, with the shorter transect affecting the top sediment layers. The fitting parameters for a piecewise CF-CS model appear in Table 2. They reveal a decrease of both, initial activity concentrations and SARs (and then in fluxes) in the recent years (the top sediment layers). As the duration of the change is relatively short (~ 20 y), the effect in the CRS chronology is only moderate, with a maximum deviation of 9 years.

Taking into account table 1, one can identify this case as a stepped change in fluxes due to changes of the same sense in A_0 and w. With the parameter values of Table 2 and the CRS chronology, used here as a first estimate of t_2 (sketch of Fig. 6a), from Eq. 16 we could expect a maximum negative deviation of ~ 13 y. This estimate is of the same sign and of the order of the one above value (from a direct comparison against the varve chronology). Depending on the final use, the researcher could consider the CRS chronology as providing a good proxy of the true one in this particular case.

Core V3: Varved sediment from Lake Zabinskie

Data from Tylmann et al. (2016). Sediment core collected in September 2011 in Lake Zabinskie at 54º07'54.50" N; 21º59'01.1" E and 44.4 m water depth. The core showed biogenic varves, and authors provided several time-marks. Those from ^{137}Cs have been used for the present study. In the above reference, authors already studied the performance of the CRS and the piecewise CF-CS models in this core. Within the scope of the present work, the core provides additional insight on the reasons for the CRS failure. A first discussion of this dataset has been presented in Fig. 2 and in the Introduction section.

The reconstructed palaeofluxes, following the methodology by Abril and Brunskill (2014), are shown in Fig. 11. It is possible to distinguish up to three regions, with increasing mean values of fluxes from the upper to the deeper sediment layers.

The Ln[$A(m)$] plot for this core (Fig. 11) shows three transects with two jump discontinuities; the first one virtually preserves the slope, while this last increases (SAR decreases) after the second discontinuity. The interpretation of the fitting parameters (Table 2) reveals an increase in the mean value of the initial activity concentration after the two transitions. Fluxes increase downcore in the three cases (Table 2) - i.e., they decreased with time (chronological dates). Thus, the above piecewise CF-CS analysis is able to capture the main features of the temporal variability in fluxes in this case, and this model provides a good proxy to the varve chronology as shown in Tylmann et al. (2016). Accounting for the magnitude of changes, their occurrence and duration (subsection 3.3 and Fig. 6, with $B < 0$), the researcher could expect a noticeable negative accumulated-deviation in the CRS chronology. Effectively, the raw CRS chronology (Fig. 2,) fails to fit the one from varves and the ^{137}Cs time marks. As also shown in Fig. 2, this discrepancy in ages cannot be satisfactorily solved with a three-transects piecewise CRS model.

Core TM4: Sediment from the Sancho Reservoir

Data from Abril et al., (2018). Sediment core sampled on late 2011 in the Sancho Reservoir, at 6°58.972'W, 37°27.697'N and at 36 m water depth. The core registered a series of major environmental changes. After the construction of the dam (on late 1962), the new sediment grew over the former floodplain with continuous and high accretion rates, interrupted by a series of depositional events, likely linked to peaks in the rainfall records. In 1972 the dam was heightened, almost doubling the capacity of the reservoir, and noticeably displacing upstream the major depositional area of riverine loads; after what the conditions for depositional events were never meet again, and SAR values progressively decreased. The reservoir has been affected by acid mine drainage, particularly since the mining cease in 2001.

The $A(m)$ profile has been truncated by omitting the depositional events (Abril et al., 2018). The resulting Ln[$A(m)$] plot for this core (Fig. 12) shows three transects with two jump discontinuities, associated to a sequential increase of A_0 from older to younger sediment layers, while SAR decreased. This last effect dominates, and the resulting fluxes onto the SWI have been decreasing with time (Table 2). As in the previous case, the researcher could expect large cumulated deviations in the CRS ages. Indeed, the CRS model chronology fails when compared with the reference dates for the construction of the dam and the heightening works (Fig. 12, panel 2).

Synthetic core S5

Abril and Brunskill (2014) studied the case of a varved sediment core from Santa Barbara Basin (data from Koide et al., 1972) for which the $^{210}Pb_{exc}$ palaeofluxes had been reconstructed (Fig. 13). They showed random variations from 1930 to 1960, followed by a continuous trend of increase that peaked around 1970, shortly before the coring. This roughly corresponds to the situation shown in Fig. 6b. The application of the CRS model also fails in this case, with positive deviation with respect to the varve chronology, as shown in Fig. 13, consistently with the theoretical analysis shown in Fig. ESM-2.

Nevertheless, this situation is more complex to detect from the analysis of a piecewise CF-CS model. First, the Ln[$A(m)$] does not allow any straightforward identification of clusters, and those shown in Fig. 13 are only tentative. It is worth noting that for the first cluster a positive linear correlation does not hold. Thus, in this case the piecewise CF-CS analysis would have failed as a warning for the application of the CRS model.

A further testing of this situation can be achieved with the synthetic core of Fig. 14. It has been built following the methodology by Abril (2016). It works with a realistic bulk density profile and with initial activity concentrations following a normal distribution with mean value of 250 Bq/kg, a relative standard deviation of 0.2, and randomly sorted in depth (time). For SAR we start from the deepest slices of the core with a normal distribution with mean value 0.18 g cm^{-2} y^{-1} and relative standard deviation of 0.15, and from midcore we linearly increase the mean value towards the SWI, resulting in the pattern of increasing fluxes shown in Fig.14. Two clusters can be distinguished, but the linear fit is poor for the upper one (Table 2). The piecewise CF-CS analysis tries to capture the mean values of the three magnitudes (A_0, w and F) for each cluster, and it concludes a sharp increase of fluxes in recent dates. From Tables 1 and 2, the researcher could conclude that the situation corresponds to a reinforced stepped increase in fluxes in recent dates. The application of Eq. 16, as a first estimate, could warn for a misapplication of the CRS model in this case, with high accumulated positive deviations in ages. Indeed, the raw CRS chronology (Fig. 14, second panel) fails to reproduce the true (synthetic) ages.

3.7. *Durbin-Watson statistic*

If e_i is the residual at sediment layer i (the difference between the observed and the predicted – from the fitting curve, value of Ln(A_i); i=1,…N), then the Durbin-Watson (DW) statistic, d, is given by

$$d = \frac{\sum_{i=2}^{N}(e_i - e_{i-1})^2}{\sum_{i=1}^{N} e_i^2} . \quad (22)$$

The value of d always lies between 0 and 4. Small values of d indicate that successive error terms are positively correlated. If $d > 2$, successive error terms are negatively correlated ($d = 2$ indicates no autocorrelation). It could be though that this statistic could be a potential indicator for the existence of distinct clusters in the whole Ln[$A(m)$] plot. Its value, along with its statistical significance, p, for the above studied cores is shown in Table 2. It takes the lowest value for core TM4, which shows three distinct clusters and the CRS chronology noticeable deviate from the reference dates. It is also below 1.0 for cores V1 and V2, where the CRS chronology is roughly acceptable. The value of d indicates weak positive autocorrelation for core V3 despite there are three distinct clusters and the CRS chronology clearly fails. Finally, no statistically significant autocorrelation is detected for core S5 for which the CRS chronology also fails. Similarly, d= 1.86 (p=0.277) for the core from Santa Barbara Basin (Fig. 13), also affected by a trend of increasing fluxes in recent dates.

4. Discussion

Results from subsection 3.1 (fluxes onto the SWI with periodic-harmonic fluctuations around the baseline value), and particularly the estimation of $\delta_{T,max}$ by Eq. 14, reveal that for relatively short periods, such as the average period length of the El Niño climatic oscillation (T_p ~5 years), $\delta_{T,max}$ is less than one year for changes in fluxes onto the SWI up to 60%. It is worth noting that a large period, of the order of several decades, makes that the oscillation in fluxes onto the SWI roughly approaches to a succession of persistent changes in environmental conditions, in such a way that decades of high fluxes follow after decades of low fluxes, and vice versa. Even in this situation, the CRS model has the ability of at least partially compensating for positive and negative deviations, and thus providing a relatively reasonable proxy to the true chronology.

Results from subsection 3.2 (fluxes onto the SWI with random variability) are promising, since this can be the type of variability in the flows of matter and activities onto the SWI which can be expected in non-perturbed sedimentary systems, likely linked to natural oscillations in climatic conditions. Consequently, the CRS chronologies are expected to show good performance in these situations, although their associated SAR histories must be handled with care, since only mean values over relative large time lapses have some physical meaning.

Results from subsection 3.3 reveal that deviations of the CRS chronologies can be unacceptable in situations in which fluxes onto the SWI show stepped variations and/or continuous trends of increase/decrease (as expected for some sedimentary systems under anthropogenic impacts). As the history of $^{210}Pb_{exc}$ fluxes onto the SWI of each studied core is not generally available, the question arises of how identifying the above unaffordable scenarios for the CRS model, whether possible, from the primary object of the chronology, namely $A(m)$. But this could be a spurious question if a piecewise CRS model could sufficiently compensate for any deviation from the true chronology. Nevertheless, this possibility has been discarded in subsection 3.4. It is worth noting that field data only can provide $A(m)$ and, when the case, the reference dates. Then, and at a first, in a piecewise CRS model there is no means to know when fluxes changed (the value of t_1 or t_2 in Fig. 6). The use of multiple reference dates likely would improve the performance of a piecewise CRS model, but there are not warranties for completely cleaning unacceptable deviations from the true chronology, as shown in the study case of Figs. 2 and 11.

In absence of any restrictive assumption for the variation of fluxes and SARs, the above persistent changes in fluxes may result untraceable in the $^{210}Pb_{exc}$ profiles, but this is possible when both magnitudes follow the statistical positive correlation found by Abril and Brunskill (2014). Thus, the analysis of clusters, along with the piecewise CF-CS model, as summarized in Table 1, has shown its use in the study of synthetic and real cores for which palaeofluxes and/or an independent chronology were available (subsections 3.5 and 3.6).

The estimation of significantly different values for the equivalent constant fluxes pre and post-dating a known reference date can serve for unambiguously identifying long-term trends of change in fluxes, as illustrated with the examples in Fig. 8. Nevertheless, the reverse is not true, and similar values for the equivalent constant fluxes may mask situations of long-term changes in fluxes, as also shown in the example of Fig. 8a (for t_r= 50y). These examples also served to illustrate how deviations from the true chronology in a piecewise CRS model decrease as the reference date approaches to the true date at which takes place the discontinuity in fluxes. Thus, it can be helpful comparing the position of the known reference dates with the discontinuities observed from a cluster analysis in the Ln[A(m)] plot.

The identification of distinct clusters in the Ln[A(m)] plot seems to be quite straightforward in some cases, but not so in others (e.g., Fig. 13). There are some mathematical tools for piecewise linear regressions, or they always can be programmed in computer codes. Nevertheless, they are subject to certain criteria (e.g., the quantification of jump discontinuities, and the threshold level for identifying a change in the slope) which also may fail in some cases.

Although the DW statistic applied to the Ln[A(m)] plot can detect some situations where the CRS model is not applicable, it fails to do so in other cases, and thus, it cannot be considered as a test of general applicability. But the same is true for the above piecewise CF-CS analysis, as shown for the case-study of Fig. 13.

In the example of Fig. 13 the application of a raw CF-CS model produces a chronology in close agreement with the one from a raw CRS model (as shown for this core in Abril and Brunskill, 2014). It is worth noting that this agreement has often been considered as a proof of consistence of the chronology, but this example well illustrates the failure of such criterion. Although ^{137}Cs data were not available for this core, as it is a varved sediment, one can use the varve-age of 1963 as a reference date to estimate the pre and post-dating constant equivalent fluxes, resulting of 662 ± 24 and 1460 ± 30 $Bq{\cdot}m^{-2}y^{-1}$, respectively. Consequently, situations in which not more than one cluster can be distinguished in the Ln[A(m)] plot can mask continuous trends of change in fluxes. Such trends of change can be revealed by the estimation of pre and post-dating constant equivalent fluxes from a known reference date. Exceptions appear in cases with long-term changes in fluxes when the used reference date is close to the age for which the two equivalent constant fluxes are equal. These ages are just those with a raw CRS δ_T ~0.

Some practical guidance can be provided after this study for continuous A(m) records and for properly truncated profiles:

i) Direct empirical evidence from varved sediments depicts a new paradigm of varying rates of supply (Fig. ESM-1). This contradicts the fundamentals of the CRS model. Nevertheless, the raw CRS model can still be a powerful tool of widespread use when the conditions for its applicability are well understood. Warnings can be linked to situations with long-term changes in $^{210}Pb_{exc}$ fluxes onto the SWI, and their proper identification becomes of capital importance. The items below assume that the studied case verifies the basic assumptions of continuity of the sequence, ideal deposition and non-posdetpositional redistribution.

ii) Independently of the adopted paradigm on fluxes, statistically-significant different values for the equivalent constant fluxes pre and post-dating a known reference date can unambiguously detect situations of long-term trends of change in fluxes.

iii) Under the paradigm of fluxes varying over time while being positively correlated with SAR (summarized in Fig. ESM-1), jump and/or slope discontinuities in the Ln[$A(m)$] plot can identify some long-term trends of change in fluxes.

iv) In the above two cases the application of a raw CRS model is not recommended, and there is not warranty that a piecewise CRS model could provide a good proxy to the true chronology. This last still can be a model choice, but being aware on the constraints shown in this study. It is possible to take some advantage from the above analysis of clusters. For instance, discrepancies in the piecewise CRS-ages are expected to reduce when the reference date is close to the observed discontinuity in the Ln[$A(m)$] plot.

v) Criteria ii) and iii) can separately fail (with false negatives) to detect some situations of long-term change in fluxes, as illustrated with examples in Fig. 8a and Fig. 13. At our present understanding, a simultaneous failure of both criteria seems to have a low probability of occurrence.

vi) A high-resolution slicing of the core and high-precision radiometric measurements can contribute to a better performance of the above tests.

vii) It can be helpful testing the consistence of the CRS outputs with the new paradigm on fluxes (Fig. ESM-1). Thus, if the computed SAR values show long-term trends of change, then results must be taken with caution, since after Fig. ESM-1, fluxes should also change according to SAR. Thus, one should be well confident that the paradigm of Abril and Brunskill (2014) does not apply in the studied case. This could be reliable in those sedimentary systems where the horizontal inputs (as defined in the above reference) are expected to be negligible.

viii) The agreement between raw CF-CS and CRS models does not prove the reliability of the chronology.

ix) In case of doubt, other models explicitly handling varying fluxes can be tested. The use of the present version of the SIT model is not recommended since it lacks of a sound physical basis. TERESA model can be a suitable option since it can solve some continuous trends of change in fluxes (e.g., it is able to produce a good proxy to the known varve-chronology in the case-study of Fig. 13, as shown in Abril, 2016).

x) Researchers should intend to extract as much information as possible from the studied core. Reference dates are of capital importance, but many other physical magnitudes can provide some insight on how the studied system behaves. Thus, among others, anomalous trends in granulometry, magnetic susceptibility, bulk density and/or the normalized profiles of activity concentrations vs mass depth of other natural radionuclides, can identify some major changes in the sedimentary conditions (e.g., see Abril et al., 2018).

xi) The radiometric dating of recent sediments is not a complete and closed body of theory. Some situations may fall beyond the present capabilities of models, and further developments may be necessary, conducted by the collective efforts of the international scientific community. Delimiting constraints and posing properly-defined problems is a logical step for this task. This thought by John A. Robbins results particularly encouraging: "When ^{210}Pb can provide chronological information it's nice but if not, it still may tell us something interesting about how a system works".

5. Conclusions

There is a wide empirical evidence in the scientific literature of that $^{210}Pb_{exc}$ fluxes onto the SWI vary with time while they are statistically correlated with SAR. This is in contradiction with the basic assumption of the most widely applied ^{210}Pb-based radiometric dating model, namely the CRS model.

For fluxes onto the SWI with periodic-harmonic or random fluctuations around the baseline value, positive and negative deviations of the CRS chronology tend to cancel out, resulting in overall acceptable chronologies. This can apply to a wide set of real cases where the short-term climatic oscillations are the major source of variability. Thus, the CRS model can still be a powerful tool of widespread use when the conditions for its applicability are well understood. Nevertheless, an acceptable model-chronology does not necessarily imply a high-resolution high-accurate SAR history, since local derivatives in the age vs mass depth curve (related with SARs) are much affected by the above fluctuations.

Persistent changes in environmental conditions resulting in a shift of the mean value of $^{210}Pb_{exc}$ fluxes onto the SWI, lead to cumulated deviations of the CRS chronology with respect to the true ages, as proved for stepped and linearly increasing *F*(t) functions . The magnitude of the maximum absolute deviation of the chronology depends on the magnitude of changes in the fluxes, the duration and age of occurrence. In these cases, the raw CRS chronology may result unacceptable.

In general, the use of a piecewise CRS model with a reference date may not satisfactorily compensate for the above deviations in chronology resulting from long-term changes in fluxes.

The new paradigm of fluxes (Abril and Brunskill, 2014), allows tracking some long-term changes in fluxes. They appear as jump and slope discontinuities in the ln[*A*(*m*)] plot when they consist in stepped changes in the mean value of SAR and/or the initial activity (Table 3.1). This has been shown with the application of a piecewise CF-CS model to some synthetic and real cases for which an independent chronology (or a set of reference dates) was available.

The analysis of clusters in the Ln[*A*(*m*)] plot, along with the estimation of equivalent constant fluxes pre and post-dating a known reference date, are powerful tools for preventing misapplications of the CRS model.

The understanding of the properties of model-errors in CRS chronologies, supported by several idealized situations and real case-studies, allows suggesting some practical guidance to prevent misapplications of the CRS model, as summarized at the end of the Discussion section.

The piecewise CRS model still can be a model choice, but being aware on the constraints shown in this study.

References

Abril J.M. (2003a) A new theoretical treatment of compaction and the advective-diffusive processes in sediments. A reviewed basis for radiometric dating models. J Paleolimnol **30**, 363–370.

Abril J.M. (2003b) Difficulties in interpreting fast mixing in the radiometric dating of sediments using ^{210}Pb and ^{137}Cs. J. Paleolimnol **30**, 407–414.

Abril J.M. (2004) Constraints on the use of Cs-137 as a timemarker to support CRS and SIT chronologies. Environ. Pollut. **129**, 31–37.

Abril J.M. (2015) Why would we use the Sediment Isotope Tomography (SIT) model to establish a ^{210}Pb-based chronology in recent-sediment cores? J. Environ. Radioact. **143**, 40-46.

Abril J.M. (2016) A ^{210}Pb-based chronological model for recent sediments with random entries of mass and activities: Model development. J. Environ. Radioact. **151**, 64-74.

Abril J.M. and Brunskil G.J. (2014) Evidence that excess ^{210}Pb flux varies with sediment accumulation rate and implications for dating recent sediments. J. Paleolimnol. **52**, 121-137.

Abril J.M. and Gharbi F. (2012) Radiometric dating of recent sediments: beyond the boundary conditions. J. Paleolimnol. **48**, 449–460.

Abril J.M., García-León M., García-Tenorio R., Sánchez C.I. and El- Daoushy F. (1992) Dating of marine sediments by an incomplete mixing model. J. Environ. Radioact. **15**,135–151.

Abril J.M., San Miguel E.G., Ruiz-Cánovas C., Casas-Ruiz M. and Bolívar J.P. (2018) From floodplain to aquatic sediments: Radiogeochronological fingerprints in a sediment core from the mining impacted Sancho Reservoir (SW Spain). Sci. Total Environ. **631–632**, 866-878. https://doi.org/10.1016/j.scitotenv.2018.03.114

Appleby P.G. (1998) Dating recent sediments by ^{210}Pb: problems and solutions. In: Illus E. (Ed) Dating of sediments and determination of sedimentation rate. STUK A-145, Finland. pp. 7–24.

Appleby P.G. (2001) Chronostratigraphic techniques in recent sediments. In: Last W.L. and Smol J.P. (Eds) Tracking environmental change using lake sediments. Basin analysis, coring, and chronological techniques. Developments in paleoenvironmental research. Kluwer, Dordrecht. pp. 171–203.

Appleby P.G. and Oldfield F. (1978) The calculation of lead-210 dates assuming a constant rate of supply of unsupported ^{210}Pb to the sediment. Catena **5**, 1–8.

Appleby P.G., Oldfield F., Thompson R., Huttunen P. and Tolonen K. (1979) Pb-210 dating of annually laminated lake sediments from Finland. Nature **280**, 53–55.

Arnaud F., Lignier V., Revel M., Desmet M., Beck C., Pourchet M., Charlet F., Trentesaux A. and Tribovillard N. (2002) Flood and earthquake disturbance of ^{210}Pb geochronology (Lake Anterne, NW Alps). Terra Nova, **14** (4), 225–232.

Binford M.W. (1990) Calculation and uncertainty analysis of ^{210}Pb dates for PIRLA project lake sediment cores. J. Paleolimnol. **3**, 253-267.

Binford M.W., Kahl J.S. and Norton S.A. (1993) Interpretation of ^{210}Pb profiles and verification of the CRS dating model in PIRLA project lake sediment cores. J. Paleolimnol. **9**, 275-296.

Botwe B.O., Abril J.M., Schirone A., Barsanti M., Delbono I., Delfanti R., Nyarko E. and Lens P.N.L. (2017) Settling fluxes and sediment accumulation rates by the combined use of sediment traps and sediment cores in Tema Harbour (Ghana). Sci. Total Environ. **609**, 1114-1125.

Carroll J. and Lerche I. (2003) Sedimentary Processes: Quantification Using Radionuclides. Elsevier, Oxford.

Christensen E.R. (1982) A model for radionuclides in sediments influenced by mixing and compaction. J. Geophys. Res. **87**, 566–572.

Chutko K.J. and Lamoureux S.F. (2009) Biolaminated sedimentation in a High Arctic freshwater lake. Sedimentology **56**, 1642–1654.

Finsinger W., Bigler Ch., Krähenbühl U., Lotter A.F. and Ammann B. (2006) Human impacts and eutrophication patterns during the past ~200 years at Lago Grande di Avigliana (N. Italy). J. Paleolimnol. **36**, 55–67.

Goldberg E.D. (1963) Geochronology with Pb-210. Proceedings of a Symposium of Radioactive Dating, International Atomic Energy Agency, Vienna. pp. 121–131.

Koide M., Soutar A. and Goldberg E.D. (1972) Marine geochronology with ^{210}Pb. Earth Planet. Sci. Lett. **14**, 442–446.

Krishnaswamy S., Lal D., Martin J.M. and Meybek M. (1971) Geochronology of lake sediments. Earth Planet. Sci. Lett. **11**, 407–414.

Klubi E., Abril J.M., Nyarko E., Laissaoui A. and Benmansour M. (2017) Radioecological assessment and radiometric dating of sediment cores from dynamic sedimentary systems of Pra and Volta estuaries (Ghana) along the Equatorial Atlantic. J. Environ. Radioact. **178-179**,116-126.

Laissaoui A., Benmansour M., Ziad N., Ibn Majah M., Abril J.M. and Mulsow S. (2008) Anthropogenic radionuclides in the water column and a sediment core from the Alboran Sea: application to radiometric dating and reconstruction of historical water column radionuclide concentration. J. Paleolimnol. **40**, 823–833.

Lamoureux S.F. (1998) Distinguishing between the geomorphic and hydro-meteorological controls recorded in clastic varved sediments. Ph D. thesis, Department of Earth and Atrnospheric Sciences, University of Alberta, Canada.

Lima A.L., Hubeny J.B., Reddy Ch.M., King J.W., Hughen K.A. and Eglinton T.I. (2005) High resolution historical records from Pettaquamscutt River basin sediments: 1. ^{210}Pb and varve chronologies validate record of ^{137}Cs released by the Chernobyl accident. Geochim. Cosmochim. Acta **69**, 1803–1812.

MacKenzie A.B. , Hardie S.M.L. , Farmer J.G., Eades L.J. and Pulford I.D. (2011) Analytical and sampling constraints in ^{210}Pb dating. Sci. Total Environ. **409**, 1298–1304.

Oldfield, F., Richardson, N., Appleby, P.G. (1995). Radiometric dating (^{210}Pb, ^{137}Cs, ^{241}Am) of recent ombrotrophic peat accumulation and evidence for changes in mass balance. The Holocene 5(2), 141-148.

Rangarajan C., Madhavan R. and Gopalakrishnan Smt S. (1986) Spatial and temporal distribution of lead-210 in the surface layers of the atmosphere. J. Environ. Radioact. **3**, 23–33.

Reinikainen P., Meriläinen J.J., Virtanen A., Veijola H. and Äystö J. (1997) Accuracy of ^{210}Pb dating in two annually laminated lake sediments with high Cs background. Appl. Radiat. Isotopes **48**, 1009–1019.

Robbins J.A. (1978) Geochemical and Geophysical applications of radioactive lead isotopes. In: Nriago JP (Ed) Biochemistry of lead in the environment. Elsevier, Amsterdam. pp. 285–393.

Robbins J.A. and Edgington D.N. (1975) Determination of recent sedimentation rates in Lake Michigan using ^{210}Pb and ^{137}Cs. Geochim. Cosmochim. Acta **39**, 285–304.

Shanahan T.M., Overpeck J.T., Beck J.W., Wheeler C.W., Peck J.A., King J.W. and Scholz Ch.A. (2008) The formation of biogeochemical laminations in Lake Bosumtwi, Ghana, and their usefulness as indicators of past environmental changes. J. Paleolimnol. **40**, 339–355.

Sánchez-Cabeza J.A. and Ruíz-Fernández A.C. (2012) ^{210}Pb sediment radiochronology: an integrated formulation and classification of dating models. Geochim. Cosmochim. Acta **82**, 183-200.

Schettler G., Mingram J., Negendank J.F.W. and Jiaqi L. (2006a) Paleovariations in the East-Asian Monsson regime geochemically recorded in varved sediments of Lake

Sihailongwan (Northeast China, Jilin province). Part 2: a 200-year record of atmospheric lead-210 flux variations and its palaeoclimatic implications. J. Paeolimnol. **35**, 271–288.

Schettler G., Qiang L., Mingram J. and Negendank J.F.W. (2006b) Paleovariations in the East-Asian Monsson regime geochemically recorded in varved sediments of Lake Sihailongwan (Northeast China, Jilin province). Part 1: Hydrological conditions and flux. J. Paleolimnol. **35**, 239–270.

Smith J.N., Boudreau B.P. and Noshkin V. (1986) Plutonium and ^{210}Pb distributions in northeast Atlantic sediments: subsurface anomalies caused by non-local mixing. Earth Planet. Sci. Lett. **81**, 15–28.

Turekian K.K., Nozaki Y. and Benninger L.K. (1977) Geochemistry of atmospheric radon and radon products. Annu. Rev. Earth Planet. Sci. **5**, 227–255.

Tylmann W., Enters D., Kinder M., Moska P., Ohlendorf Ch., Poreba G. and Zolitschka B. (2013) Multiple dating of varved sediments from Lake Łazduny, northern Poland: toward an improved chronology for the last 150 years. Quat. Geochronol .**15**, 98–107.

Tylmann W., Alicja Bonk A., Goslar T., Wulf S. and Grosjean M. (2016) Calibrating ^{210}Pb dating results with varve chronology and independent chronostratigraphic markers: Problems and implications. Quaternary Geochronology **32**, 1-10.

Wan G.J., Santschi P.H., Sturm M., Farrenkothen K., Lueck A.,Werth E. and Schuler Ch. (1987) Natural (^{210}Pb, ^{7}Be) and fallout (^{137}Cs, ^{239,240}Pu, ^{90}Sr) radionuclides as geochemical tracers of sedimentation in Greifensee, Switzerland. Chem. Geol. **63**, 181–196.

Winkler R. and Rosner G. (2000) Seasonal and long-term variation of ^{210}Pb concentration in air, atmospheric deposition rate and total deposition velocity in south Germany. Sci. Total Environ. **263**, 57–68.

FIGURE CAPTIONS

Figure 1. Sketch of the ^{210}Pb-based radiometric dating problem (upper panel): In absence of restrictive assumptions else than ideal deposition, continuity of the sequence and non-postdepositional redistribution, any $^{210}Pb_{exc}$ vs mass depth (*m*) profile is compatible with an infinite number of chronological lines (three are depicted), each one defining a particular history for SARs and palaeofluxes onto the SWI. The second panel shows a detail of the true and model chronological lines, illustrating spurious SARs (related with the local derivative) associated to a partial or approximate accomplishment of the model assumptions.

Figure 2. First panel: $^{210}Pb_{exc}$ vs. mass depth profile for a varved sediment from Lake Zabinskie (data from Tylmann et al., 2016), along with the chronologies obtained from a raw CRS model, and from the piecewise CRS model when using one and two reference dates (1963 and 1986, from ^{137}Cs data). The second panel shows the deviations of the above piecewise-CRS chronologies from the known chronology from varves (after Tylmann et al., 2016). Error-bars are 1σ propagated uncertainties. For the sake of comparison, this panel also depicts the deviation of a chronology built as a linear interpolation among the origin and the two known reference dates.

Figure 3. Sketch of a piecewise CF-CS model applied to a Ln[$A(m)$] plot with three clusters delimited by jump discontinuities with changes in the slope. Mean values for SARs and the initial activity concentrations can be estimated from the slopes and the ordinates in the origin (Eqs. 9 to 11). Dispersion in data arises from random variations around the mean values of A_0 and w.

Figure 4. Analytical solutions for the deviation in the CRS chronology under fluxes onto the SWI with periodic-harmonic fluctuations around a baseline value (Eq. 12, with F_0= 100 Bq·m^{-2}y^{-1}). They are depicted for different values of the amplitude of the oscillation (B, in Bq·m^{-2}y^{-1}), its period (T_p, in years), and the phase (φ, in radians).

Figure 5. Synthetic $^{210}Pb_{exc}$ vs mass depth (*m*) profile (first panel) generated with $^{210}Pb_{exc}$ fluxes and SARs with a random variability (second panel). The CRS

chronology (first panel) and SARs (second panel) are depicted along with the corresponding true (synthetic) values.

Figure 6. Sketch with two types of temporal variability of $^{210}Pb_{exc}$ fluxes onto the SWI, $F(t)$.

Figure 7. Analytical solutions for the deviation in the CRS chronology under fluxes with stepped variations (Fig. 6a). They are depicted for different values of the jump discontinuity (B, in $Bq \cdot m^{-2} y^{-1}$), the duration (DT= t_2-t_1) and the age t_1, both given in years. In all the cases F_0= 100 $Bq \cdot m^{-2} y^{-1}$.

Figure 8. Computed deviations of the piecewise CRS chronologies for three cases of $F(t)$ given by Fig. 6a (parameter values are given at each panel). A single reference date, t_r, is used in all the cases, but the modelling exercise is repeated for three different values of t_r, as indicated in each panel.

Figure 9. Ln[$A(m)$] plot (first panel) for Core V1, a varved sediment from Pettaquamscutt River basin (data from Lima et al., 2005). The fitting parameters for lines r_1 and r_2 are shown in Table 2. The reconstructed records of palaeofluxes are also plotted. The raw CRS chronology is depicted along with the one derived from varves (second panel).

Figure 10. Ln[$A(m)$] plot (first panel) for Core V2, a varved sediment from Sihailongwan Lake (data from Schettler et al., 2006a, and truncated by the depositional event registered in its slice number 5). The fitting parameters for lines r_1 and r_2 are shown in Table 2. The reconstructed records of palaeofluxes are also plotted. The CRS chronology is depicted along with the one derived from varves (second panel).

Figure 11. Ln[$A(m)$] plot (first panel) for Core V3, a varved sediment from Lake Zabinskie (data from Tylmann et al., 2016). The fitting parameters for lines r_1, r_2 and r_3 are shown in Table 2. The reconstructed records of palaeofluxes are also plotted. Several CRS-based chronologies are shown in Fig. 2.

Figure 12. Ln[$A(m)$] plot (first panel) for Core TM4, a sediment from the Sancho Reservoir (data from Abril et al., 2018). The fitting parameters for lines $r_{1,}$ r_2 and r_3 are shown in Table 2.The CRS chronology is depicted along with two time marks (second panel).

Figure 13. Ln[$A(m)$] plot (first panel) for a varved sediment from Santa Barbara Basin (data from Koide et al., 1972), along with palaeofluxes reconstructed by Abril and Brunskill (2014). The separation of several clusters is not justified in this case, and the selected ones are only for illustration purposes. The CRS chronology is depicted along with the varve ages (second panel).

Figure 14. Ln[$A(m)$] plot (first panel) for Core S5, a synthetic core generated with random values of initial activity concentration (normal distribution with mean value 250 Bq/kg and relative standard deviation of 0.20), and SAR with random variations and increasing mean value towards the SWI, resulting in the varying fluxes shown in the first panel. The fitting parameters for lines $r_{1,}$ and r_2 are shown in Table 2.The CRS chronology is depicted along with the synthetic ages (second panel).

FIGURE CAPTIONS FOR ELECTRONIC SUPPLEMENTARY MATERIAL

Figure ESM-1 Frequency distributions (left panels) for normalized (to the arithmetic mean of each core) initial activities, and SAR with data from 149 slices from 9 varved sediment cores from marine, riverine a wide diversity of lacustrine environments (Abril and Brunskill, 2014). The continuous line plots the normal distribution for the sake of comparison. Panels on the right show normalized $^{210}Pb_{exc}$ fluxes and initial activity concentrations versus normalized SAR, and linear BCES ((Bivariate Correlated Errors and intrinsic Scatter) regression. Normalization refers to the arithmetic mean value of the magnitude in each sediment core. These statistical features also hold for each single core (Abril and Brunskill, 2014).

Figure ESM-2. Analytical solutions for the deviation in the CRS chronology under fluxes with a continuous trend of increase/decrease (Fig. 6b). They are depicted for different values of B (in Bq·m^{-2}y^{-1}) and t_1 (in years). In all the cases F_0= 100 Bq·m^{-2}y^{-1}. Deviations of the CRS chronology, $\delta_T(t_m)$, have been estimated by Eq. 3, with $\Sigma_m = \frac{F_0}{\lambda} e^{-\lambda t_1} + \frac{B+F_0}{\lambda}\left(e^{-\lambda t_m} - e^{-\lambda t_1}\right) - \frac{B}{t_1\lambda^2}\left[-\lambda t e^{-\lambda t} - e^{-\lambda t}\right]_{t_m}^{t_1}$ for $t_m < t_1$ and $\Sigma_m = \frac{F_0}{\lambda}e^{-\lambda t_m}$ for $t_m < t_1$.

Table 1. Effects of temporal changes in initial activity concentrations, A_o, and SARs (in the sense of growing ages –i.e., increasing m) in the Ln[$A(m)$] plot, and their implications for ^{210}Pb fluxes onto the SWI and on the applicability of the CRS model.

Changes in A_o	Changes in SAR	Effect in the Ln[$A(m)$] plot	Fluxes	CRS applicability
Random variations	Random variations	Dispersion around trend-line	Random variation	Possible
Negative (a)/positive (b) shift in mean value	Random variations	Negative(a)/positive(b) jump discontinuity without change in slope	Negative (a)/positive (b) shift in mean value	Cumulated deviation in ages
Random variations	Negative (c)/ positive (d) shift in mean value	Discontinuity in slope: increase (c)/decrease (d)	Negative (c)/ positive (d) shift in mean value	Cumulated deviation in ages
Negative/positive shift in mean value	Negative/positive shift in mean value	Negative/positive jump discontinuity and the slope increases /decreases.	Reinforced negative/ positive shifts in mean value	Cumulated deviation in ages
Positive (e)/negative (f) shift in mean value	Negative (e)/positive (f) shift in mean value	Positive (e)/negative (f) jump discontinuity and the slope increases (e) / decreases (f)	Depending on the magnitude of each change, fluxes could remain unchanged	Quantify fluxes from CF-CS model before applying CRS

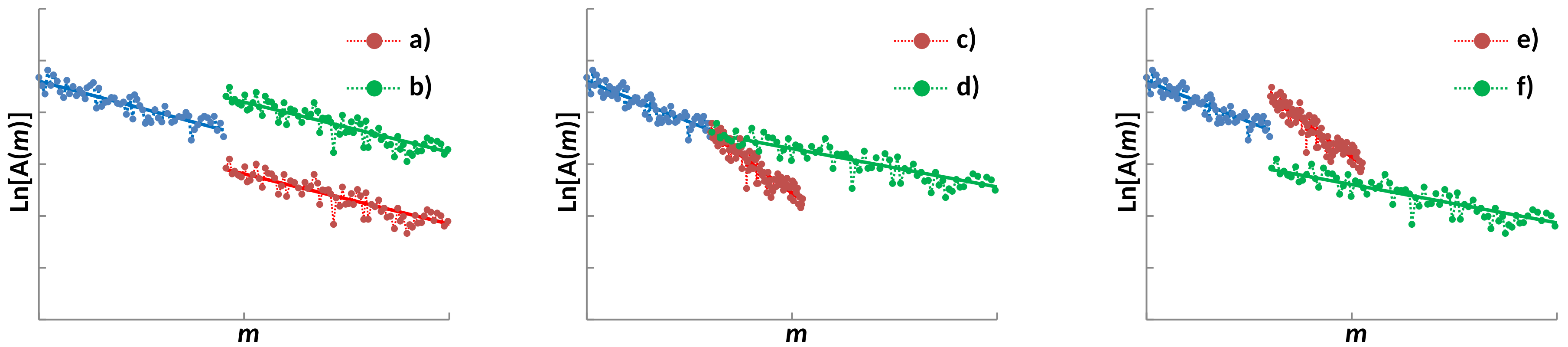

Letters in brackes refer to the reference plots, which are shown as examples. They have been built with A_0 =100 Bq/kg and w =0.30 g·cm^{-2}y^{-1} for the reference (blue) line, both with 15% of relative standard deviation. Clusters a) and b) keep the same w but with half and double value of A_0, respectively; clusters c) and d) keeps the value of A_0 with half and double value of w, respectively; clusters e) and f) keep the flux constant with double and half values for A_0 and w, and viceversa, respectively.

Table 2. Fitting parameters for a piecewise CF-CS model, and estimation of $^{210}Pb_{exc}$ fluxes for the studied set of sediment cores.

Parameter	Core V1 [1]	Core V2 [2]	Core V3 [3]	Core TM4 [4]	Core S5 [5]
$-s_1$	0.401 ± 0.027	4.0 ± 0.8	0.273 ± 0.016	0.79 ± 0.14	0.060 ± 0.024
b_1	6.16 ± 0.05	7.91 ± 0.08	5.71 ± 0.04	4.76 ± 0.06	5.47 ± 0.11
m_1	3.91	0.26	4.89	0.75	8.28
$-s_2$	0.99 ± 0.06	1.58 ± 0.03	0.232 ± 0.017	0.322 ± 0.012	0.165 ± 0.017
b_2	5.08 ± 0.13	7.07 ± 0.06	4.98 ± 0.07	3.99 ± 0.03	5.92 ± 0.23
m_2			11.94	5.55	
$-s_3$			0.32 ± 0.08	0.066 ± 0.027	
b_3			3.98 ± 0.15	2.91 ± 0.18	
$Ao,_1$	474 ± 25	2720 ± 220	301 ± 12	117 ± 7	240 ± 25
w_1	0.068 ± 0.004	0.0077 ± 0.0015	0.114 ± 0.007	0.039 ± 0.007	0.51 ± 0.20
$Ao,_2$	950 ± 160	3400 ± 700	550 ± 60	98 ± 11	160 ± 40
w_2	0.031 ± 0.002	0.0198 ± 0.0003	0.134 ± 0.010	0.096 ± 0.004	0.189 ± 0.019
$Ao,_3$			2000 ± 400	46 ± 10	
w_3			0.096 ± 0.025	0.47 ± 0.20	
F_1	323 ± 26	210 ± 40	343 ± 25	46 ± 8	1200 ± 500
F_2	300 ± 50	670 ± 140	740 ± 90	95 ± 11	300 ± 70
F_3			1900 ± 600	220 ± 100	
DW	0.98 (**0.0017**)	0.84 (**0.0007**)	1.44 (**0.019**)	0.41 (**0.000**)	1.67 (0.13)

In the Ln[$A(m)$] plots, $A(m)$ is given in Bq·kg^{-1} and m in g·cm^{-2}. $A_{o,i}$ and w_i (i=1,2,3 –it refers to transects or clusters) have units of Bq·kg^{-1} and g·cm^{-2}y^{-1}, respectively, and F_i are given in Bq·m^{-2}y^{-1}; s_i are slopes, and b_i the independent terms in the linear fit. Values and errors in $A_{o,i}$ for i>1have been estimated from Ln[$A(m')$] plots with a translation to the origin ($m' = m-m_1$ for i=2; $m' = m-m_2$ for i=3).

DW: Durbin-Watson statistic for the whole Ln[$A(m)$] plots (in parentheses the p value)

[1] Plot in Fig. 9, data from Lima et al. (2005); [2] Plot in Fig. 10, data from Schettler et al. (2006) by excluding slice number 5; [3] Plot in Fig. 11, data from Tylmann et al. (2016); [4] Plot in Fig. 12, data from Abril et al. (2018); [5] Plot in Fig. 14, synthetic core (see text).

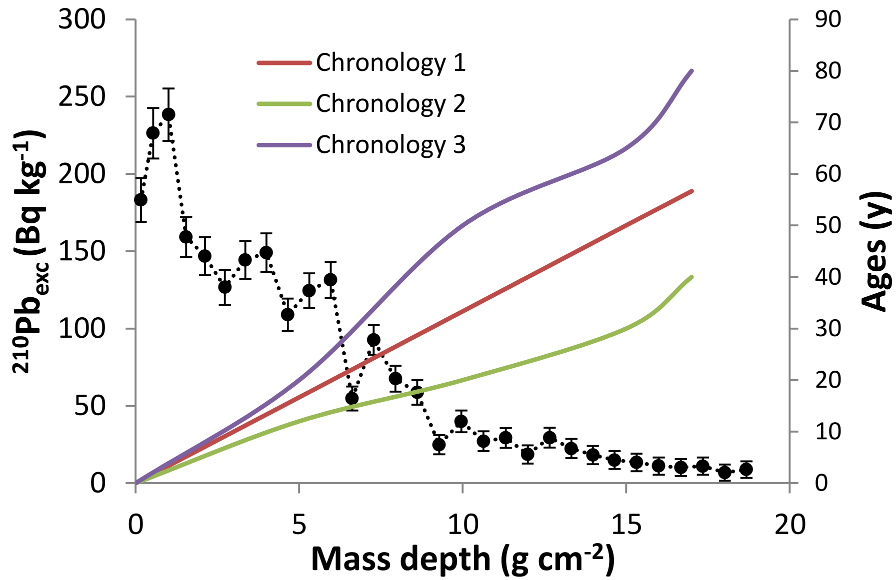
300
250
200
150
100
50
0
90
80
70
60
50
40
30
20
10
0
0
5
10
15
20
Chronology 1
Chronology 2
Chronology 3
$^{210}Pb_{exc}$ (Bq kg^{-1})
Ages (y)
Mass depth (g cm^{-2})

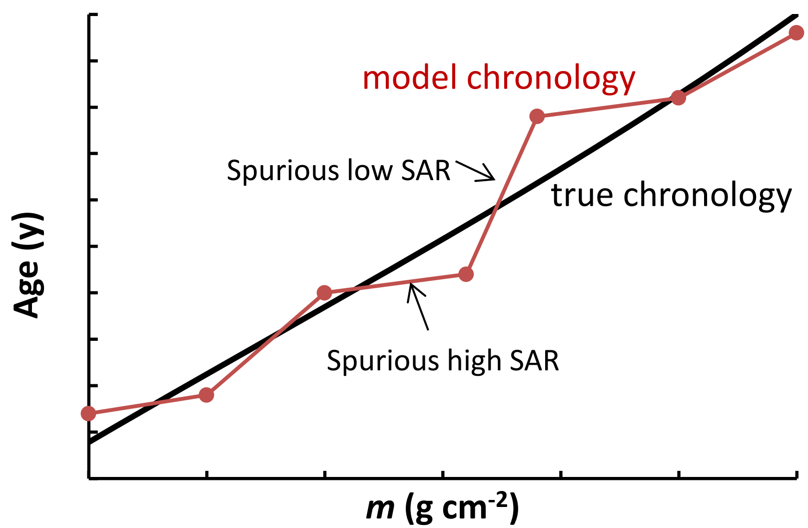
model chronology
Spurious low SAR
true chronology
Spurious high SAR
Age (y)
m (g cm^{-2})

Fig. 1

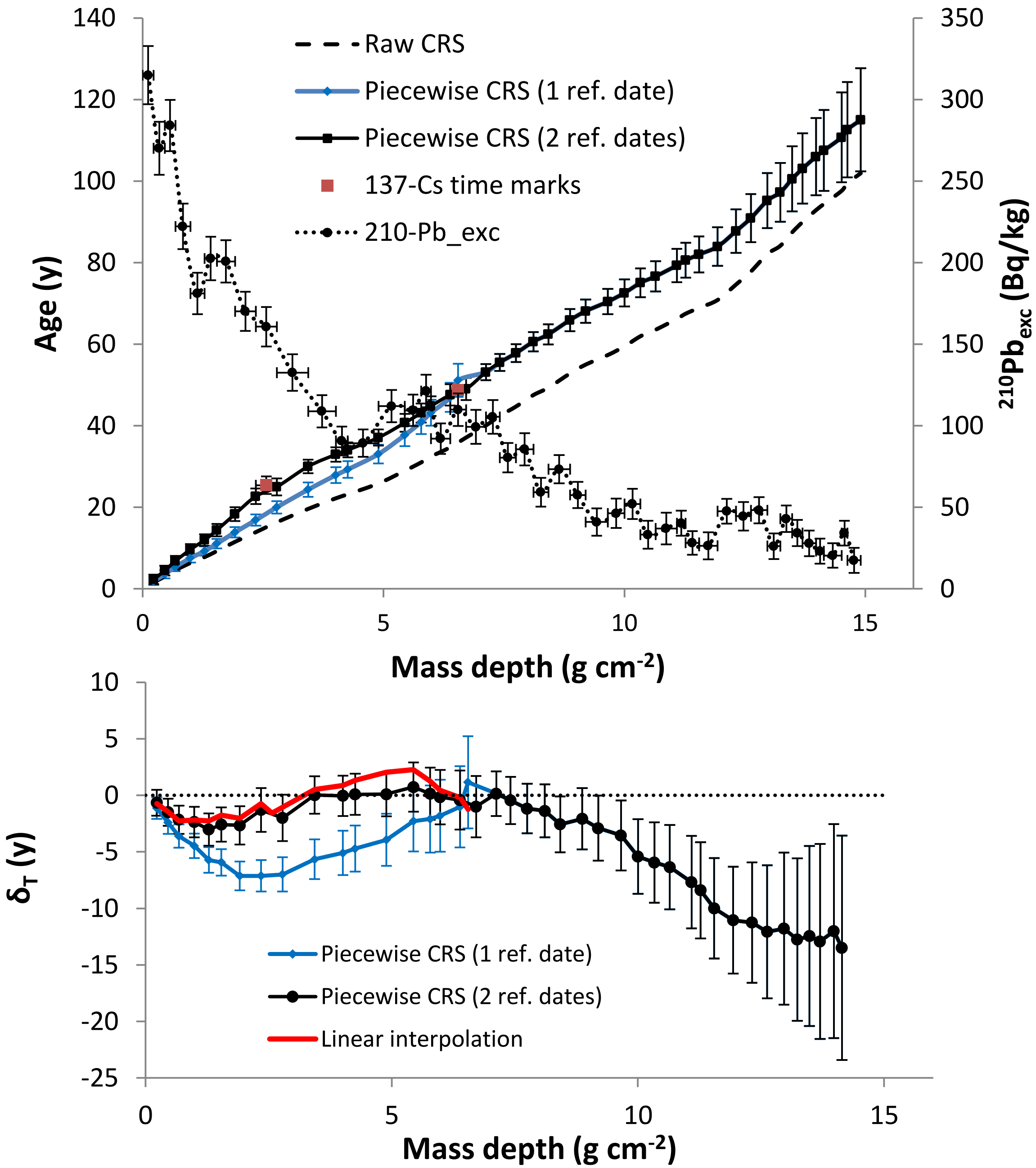

140
120
100
80
60
40
20
0
350
300
250
200
150
100
50
0
Raw CRS
Piecewise CRS (1 ref. date)
Piecewise CRS (2 ref. dates)
137-Cs time marks
210-Pb_exc
Age (y)
$^{210}Pb_{exc}$ (Bq/kg)
0
5
10
15
Mass depth (g cm^{-2})
10
5
0
-5
-10
-15
-20
-25
δ_T (y)
Piecewise CRS (1 ref. date)
Piecewise CRS (2 ref. dates)
Linear interpolation
0
5
10
15
Mass depth (g cm^{-2})

Fig. 2

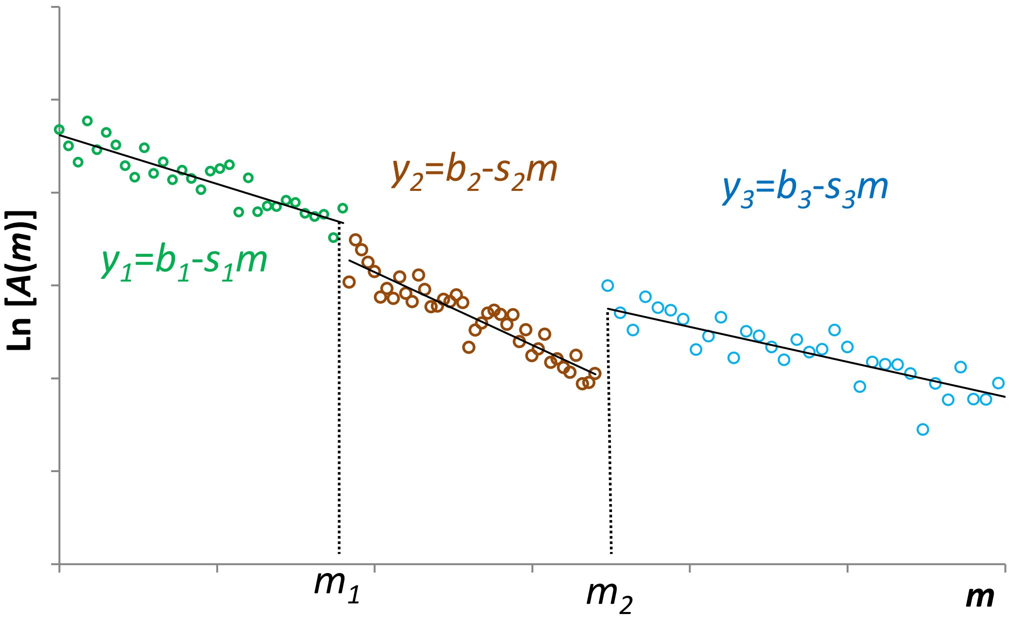

Fig. 3

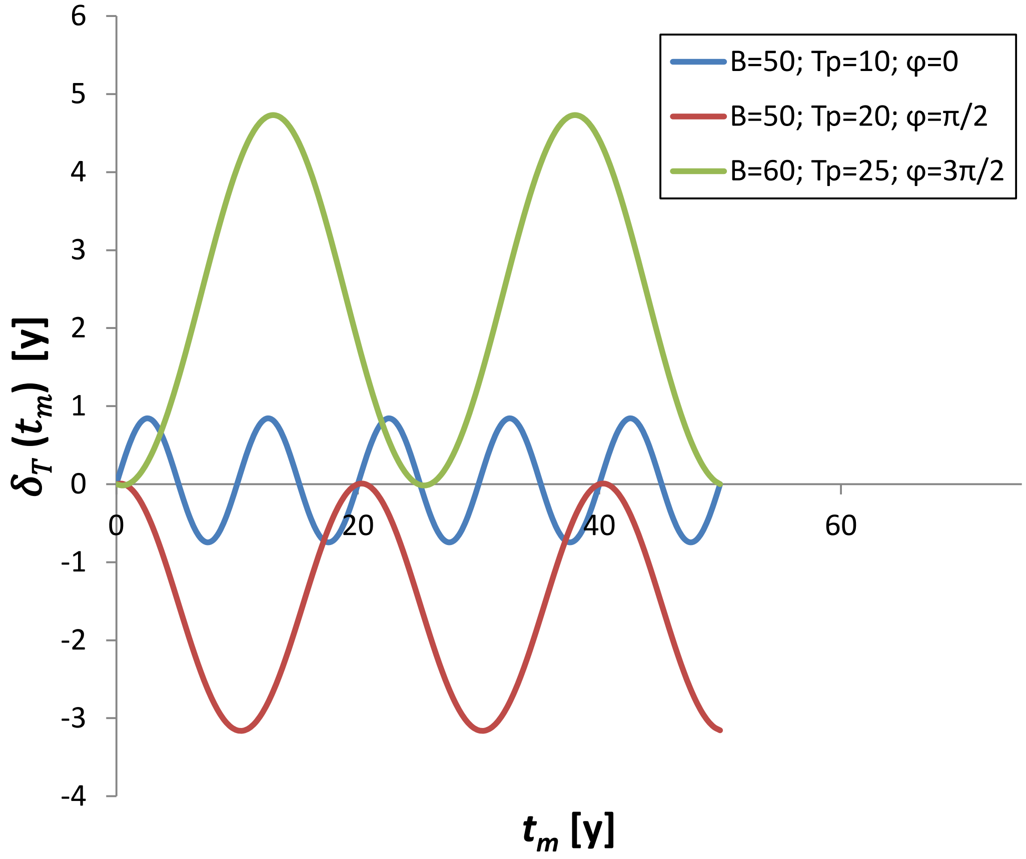

B=50; Tp=10; φ=0
B=50; Tp=20; φ=π/2
B=60; Tp=25; φ=3π/2
6
5
4
3
2
1
0
-1
-2
-3
-4
0
20
40
60
$\delta_T\ (t_m)$ [y]
t_m [y]

Fig. 4

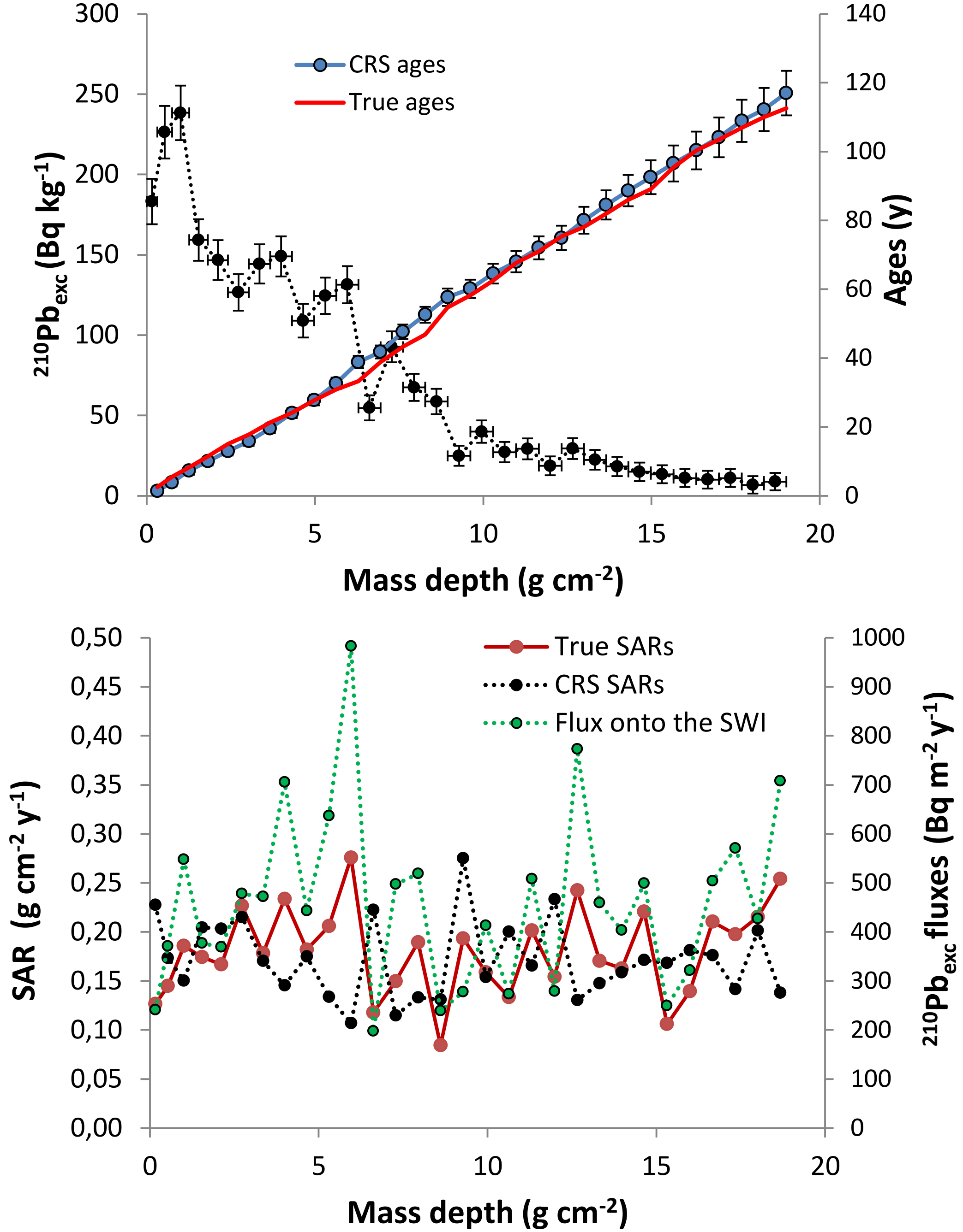

CRS ages
True ages
$^{210}Pb_{exc}$ (Bq kg^{-1})
Ages (y)
Mass depth (g cm^{-2})
True SARs
CRS SARs
Flux onto the SWI
SAR (g cm^{-2} y^{-1})
$^{210}Pb_{exc}$ fluxes (Bq m^{-2} y^{-1})
Mass depth (g cm^{-2})

Fig. 5

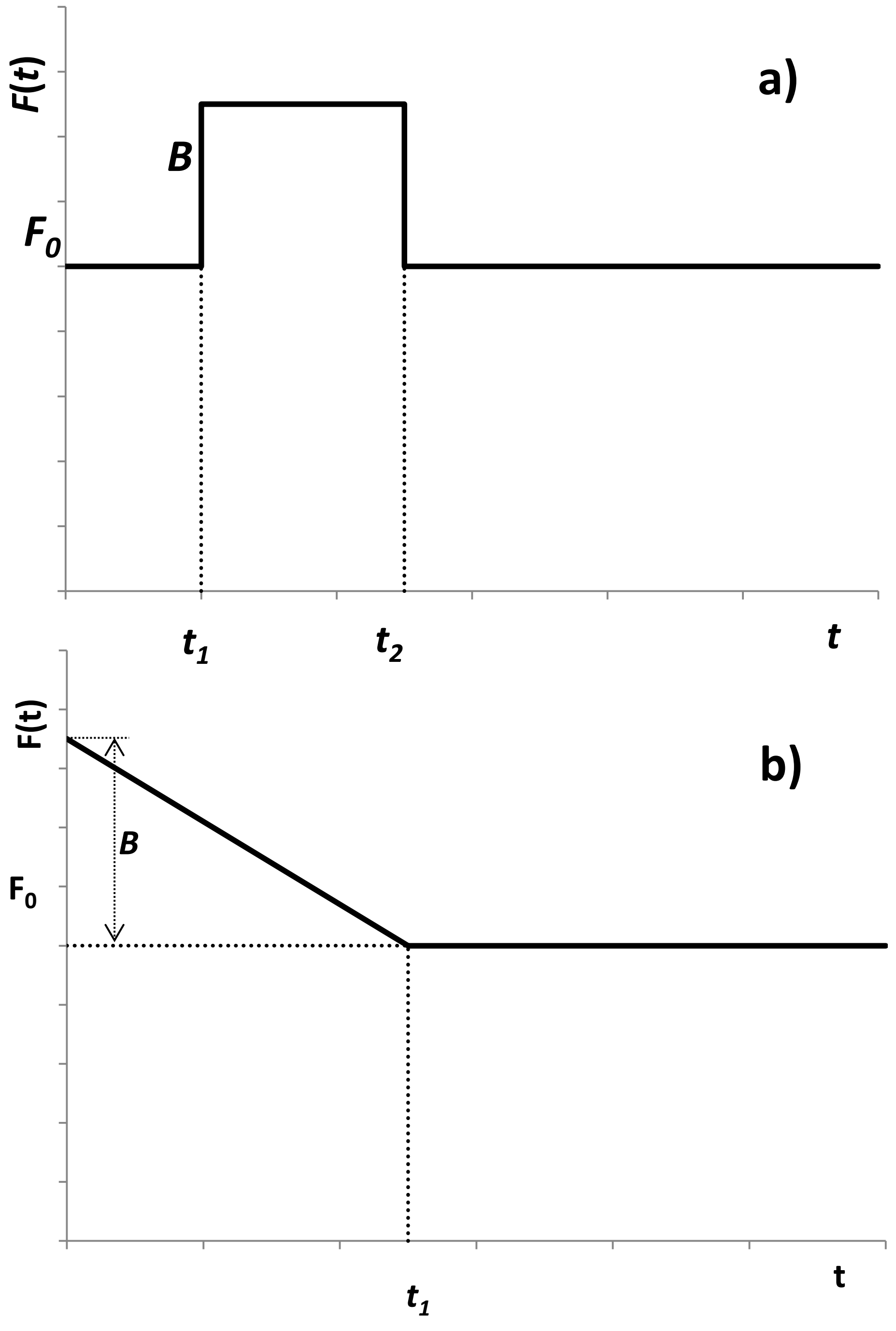

Fig. 6

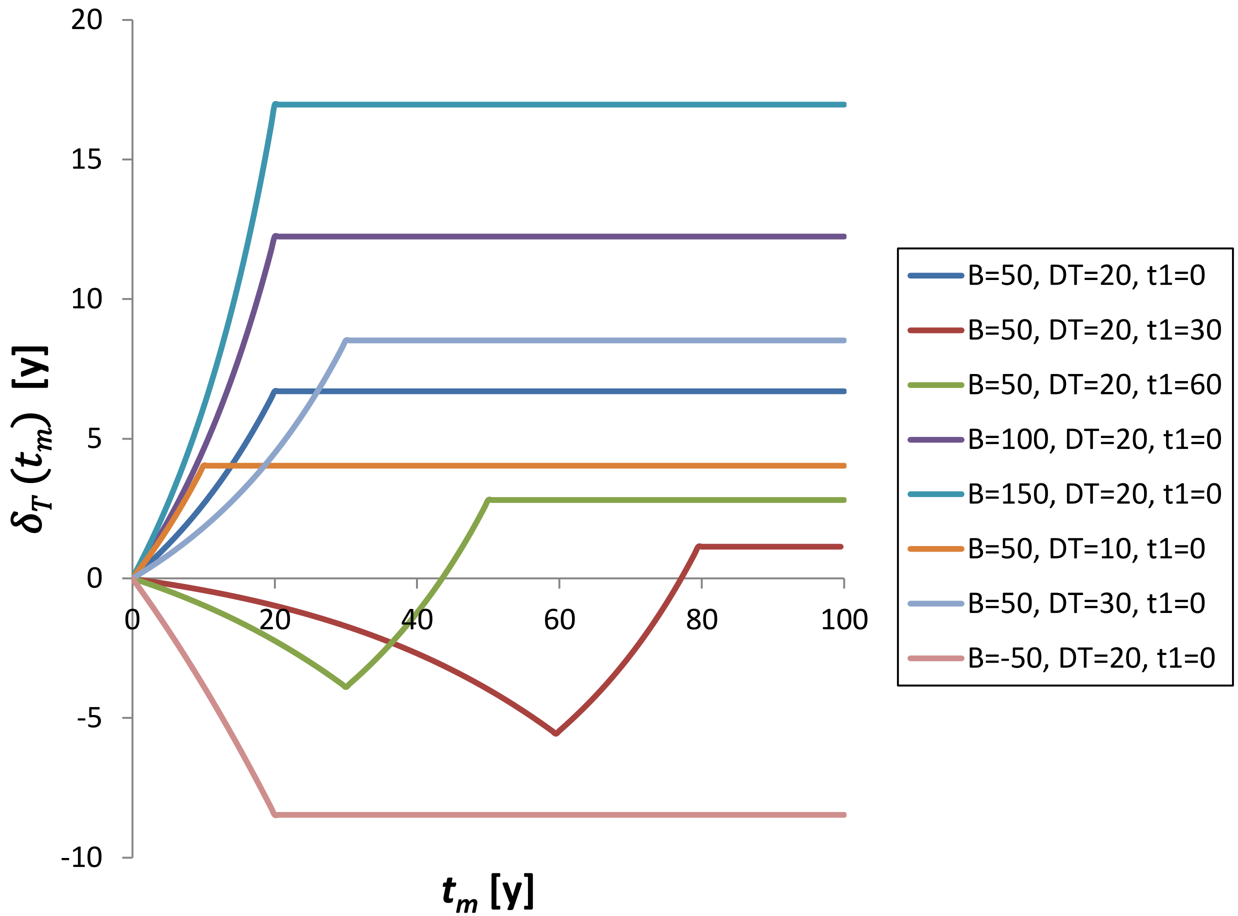

20
15
10
5
0
-5
-10
0
20
40
60
80
100
$\delta_T\,(t_m)$ [y]
t_m [y]
B=50, DT=20, t1=0
B=50, DT=20, t1=30
B=50, DT=20, t1=60
B=100, DT=20, t1=0
B=150, DT=20, t1=0
B=50, DT=10, t1=0
B=50, DT=30, t1=0
B=-50, DT=20, t1=0

Fig. 7

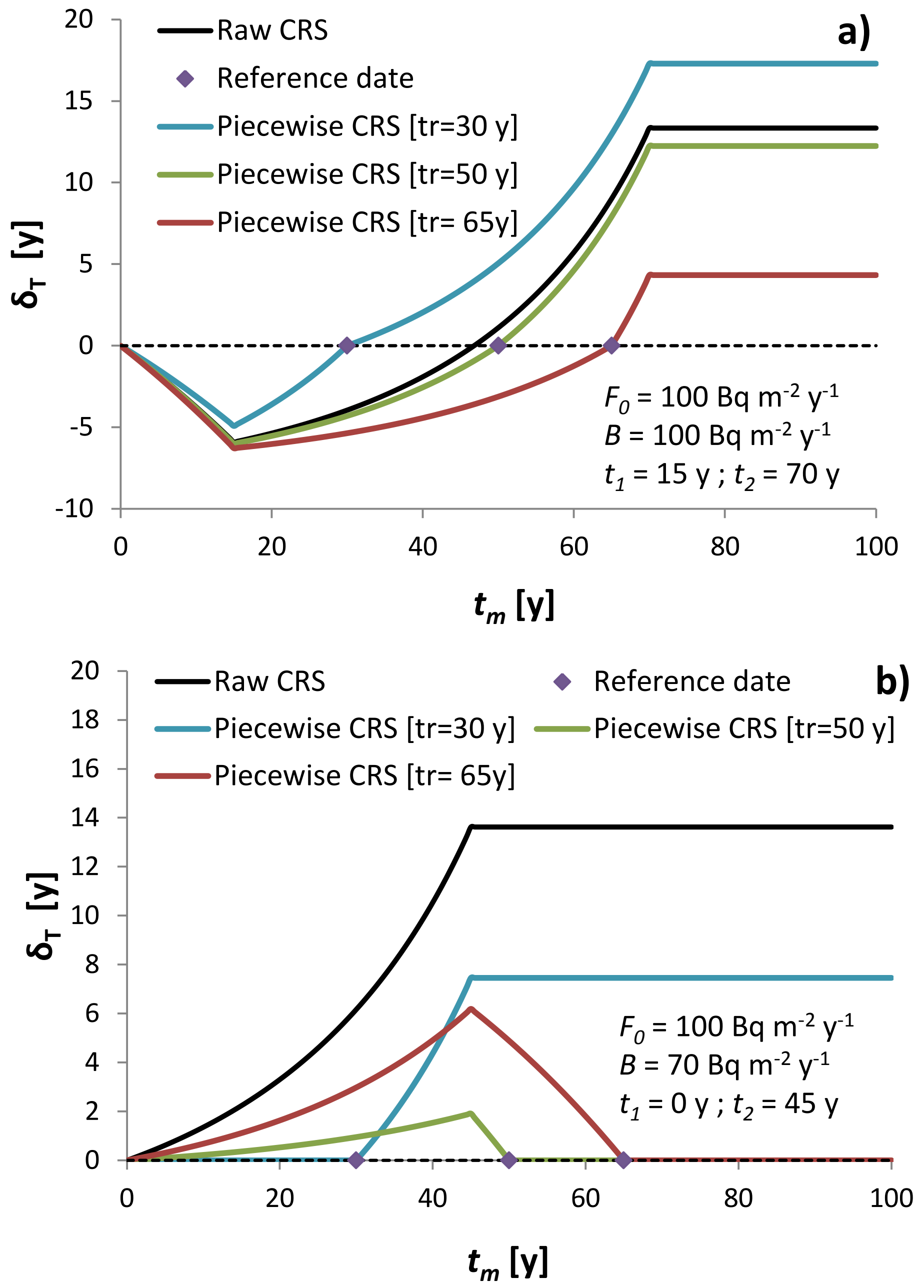

a)
Raw CRS
Reference date
Piecewise CRS [tr=30 y]
Piecewise CRS [tr=50 y]
Piecewise CRS [tr= 65y]
δT [y]
tm [y]
F0 = 100 Bq m-2 y-1
B = 100 Bq m-2 y-1
t1 = 15 y ; t2 = 70 y
b)
Raw CRS
Reference date
Piecewise CRS [tr=30 y]
Piecewise CRS [tr=50 y]
Piecewise CRS [tr= 65y]
δT [y]
tm [y]
F0 = 100 Bq m-2 y-1
B = 70 Bq m-2 y-1
t1 = 0 y ; t2 = 45 y

Fig. 8

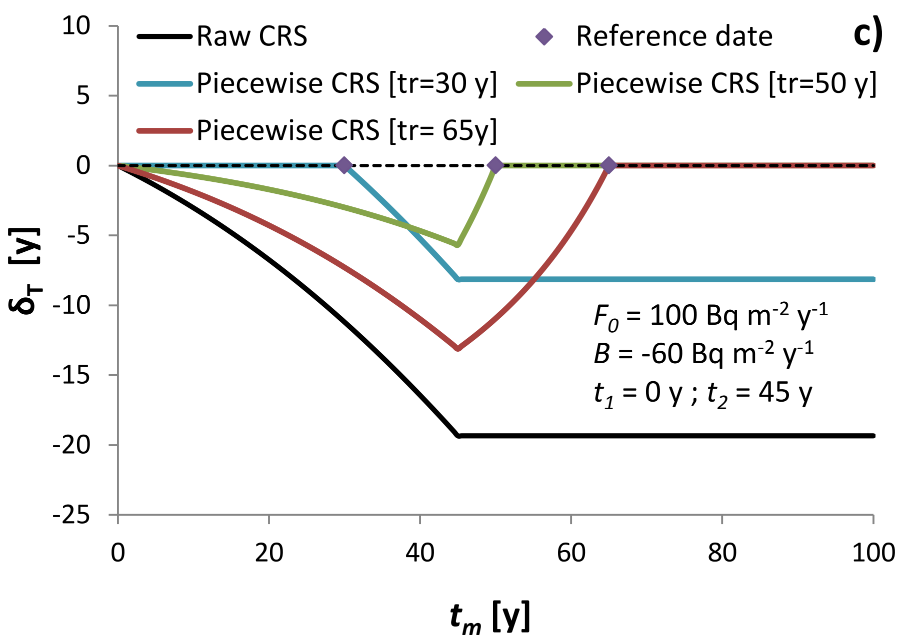

Fig. 8 (continuation)

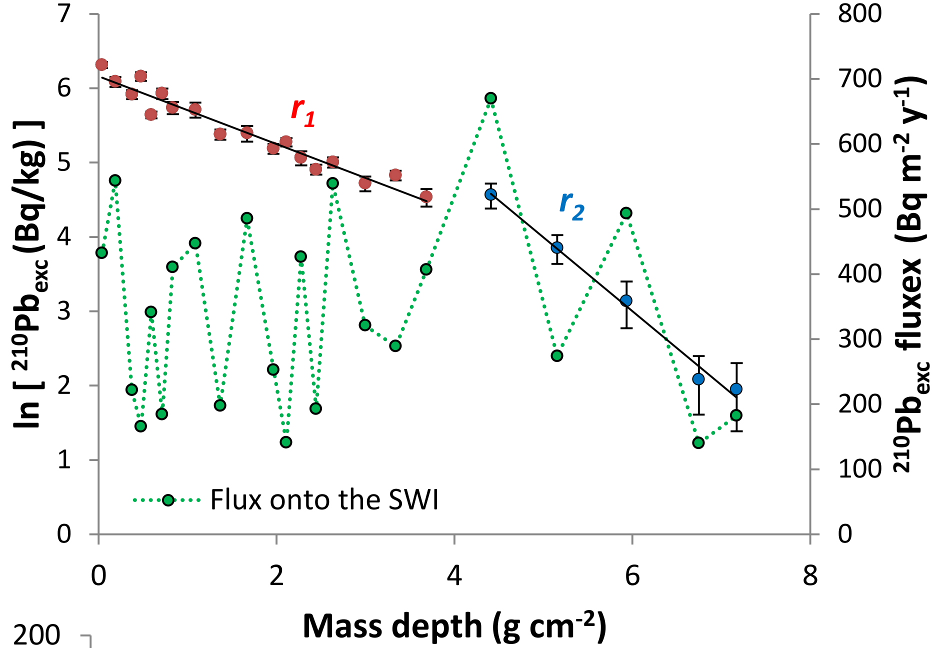

7
6
5
4
3
2
1
0
800
700
600
500
400
300
200
100
0
ln [$^{210}Pb_{exc}$ (Bq/kg)]
$^{210}Pb_{exc}$ fluxex (Bq m^{-2} y^{-1})
r_1
r_2
Flux onto the SWI
0
2
4
6
8
Mass depth (g cm^{-2})

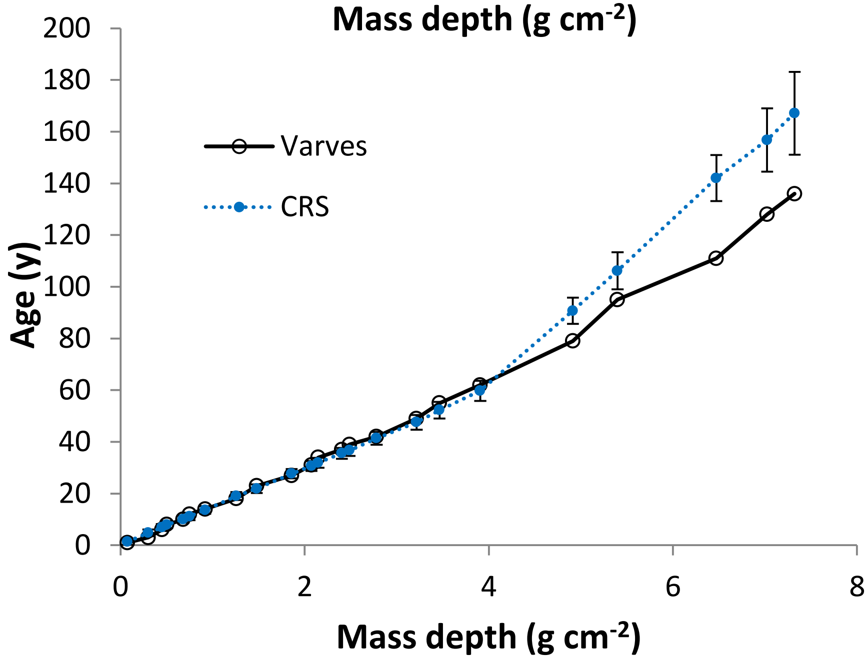

200
180
160
140
120
100
80
60
40
20
0
Age (y)
Varves
CRS
0
2
4
6
8
Mass depth (g cm^{-2})

Fig. 9

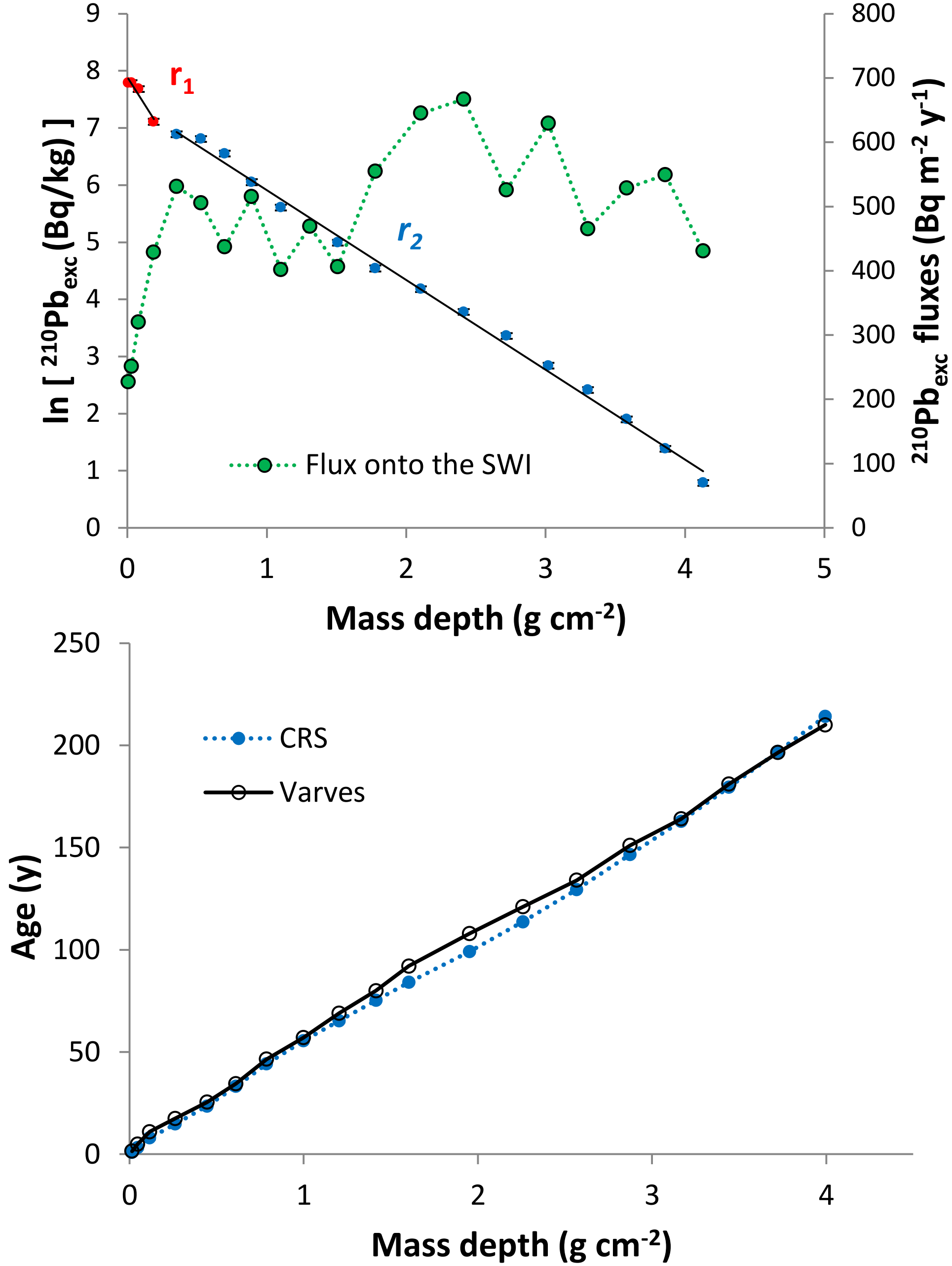
r1
r2
Flux onto the SWI
ln [$^{210}Pb_{exc}$ (Bq/kg)]
$^{210}Pb_{exc}$ fluxes (Bq m^{-2} y^{-1})
Mass depth (g cm^{-2})
CRS
Varves
Age (y)
Mass depth (g cm^{-2})

Fig. 10

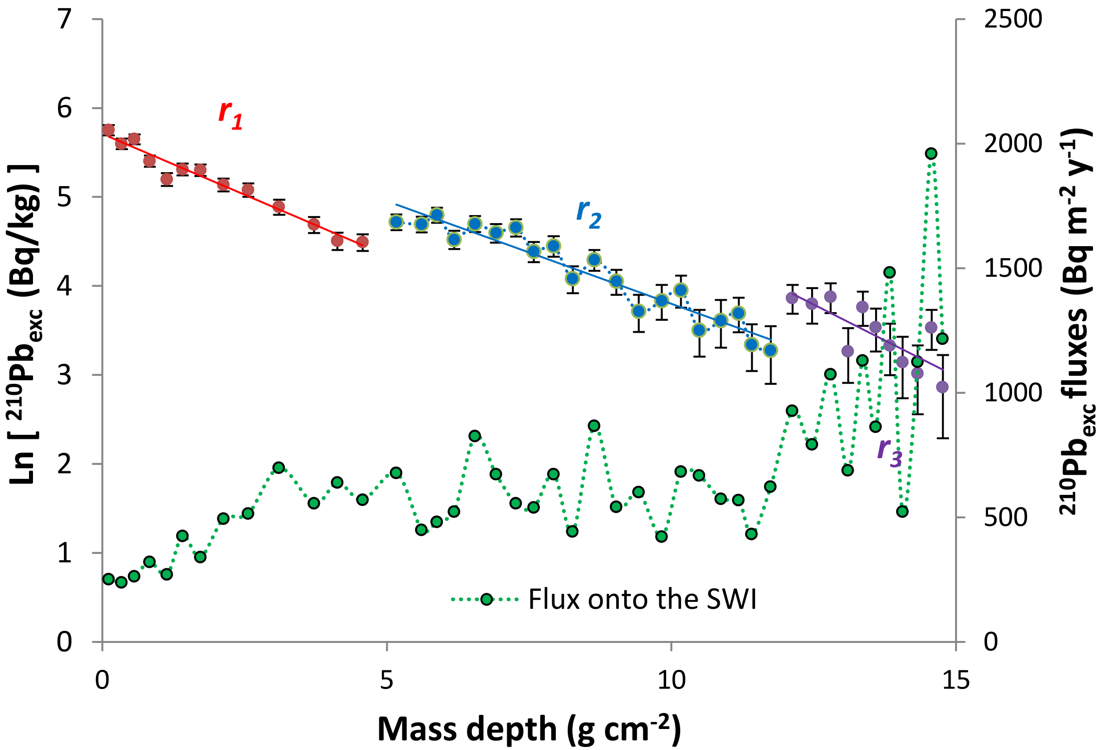
r1
r2
r3
Ln [210Pbexc (Bq/kg)]
210Pbexc fluxes (Bq m-2 y-1)
Mass depth (g cm-2)
Flux onto the SWI
0
1
2
3
4
5
6
7
0
5
10
15
0
500
1000
1500
2000
2500

Fig. 11

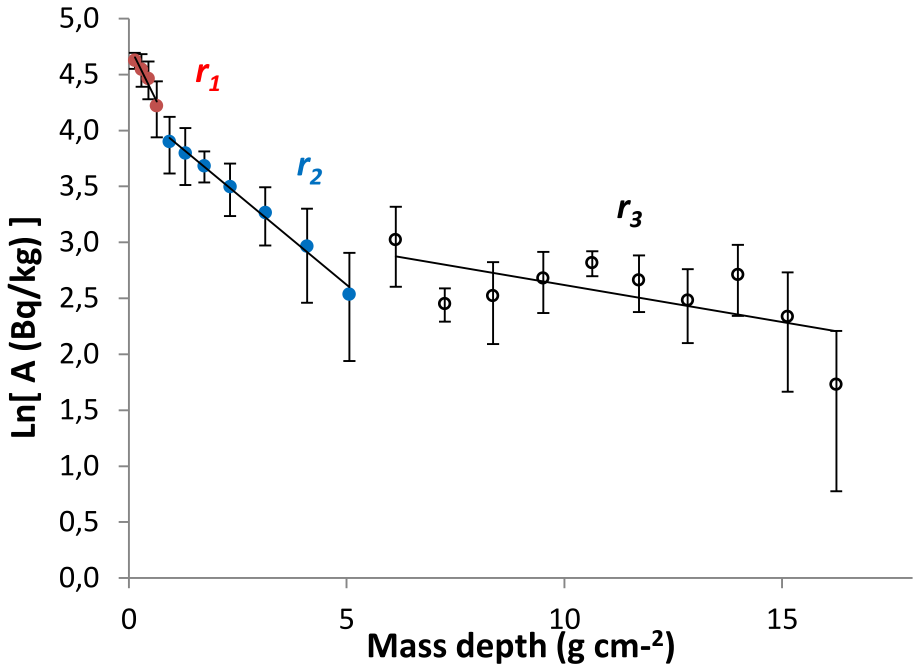

5,0
4,5
4,0
3,5
3,0
2,5
2,0
1,5
1,0
0,5
0,0
Ln[A (Bq/kg)]
r1
r2
r3
0
5
10
15
Mass depth (g cm-2)

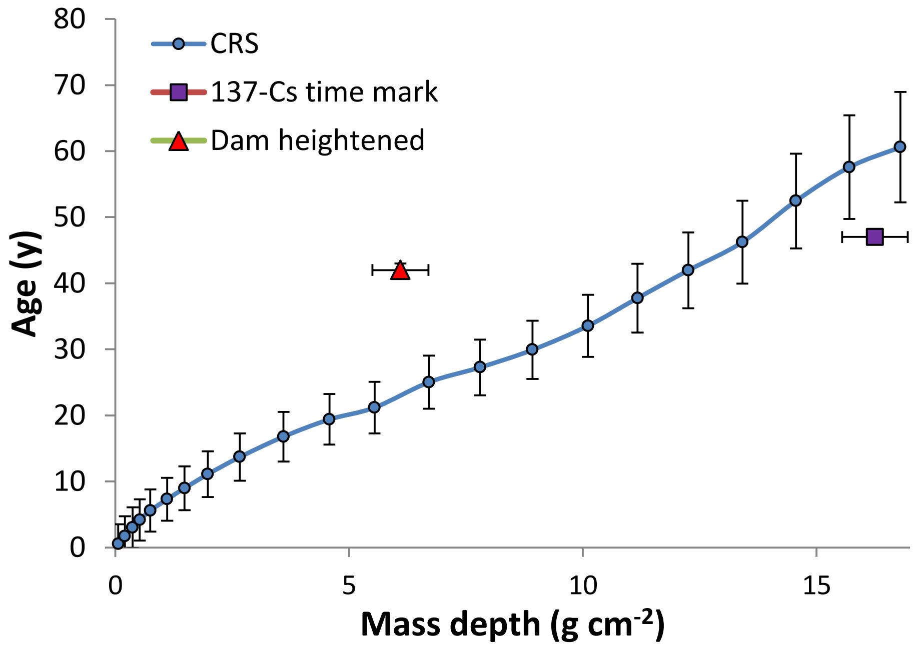

80
70
60
50
40
30
20
10
0
Age (y)
CRS
137-Cs time mark
Dam heightened
0
5
10
15
Mass depth (g cm-2)

Fig. 12

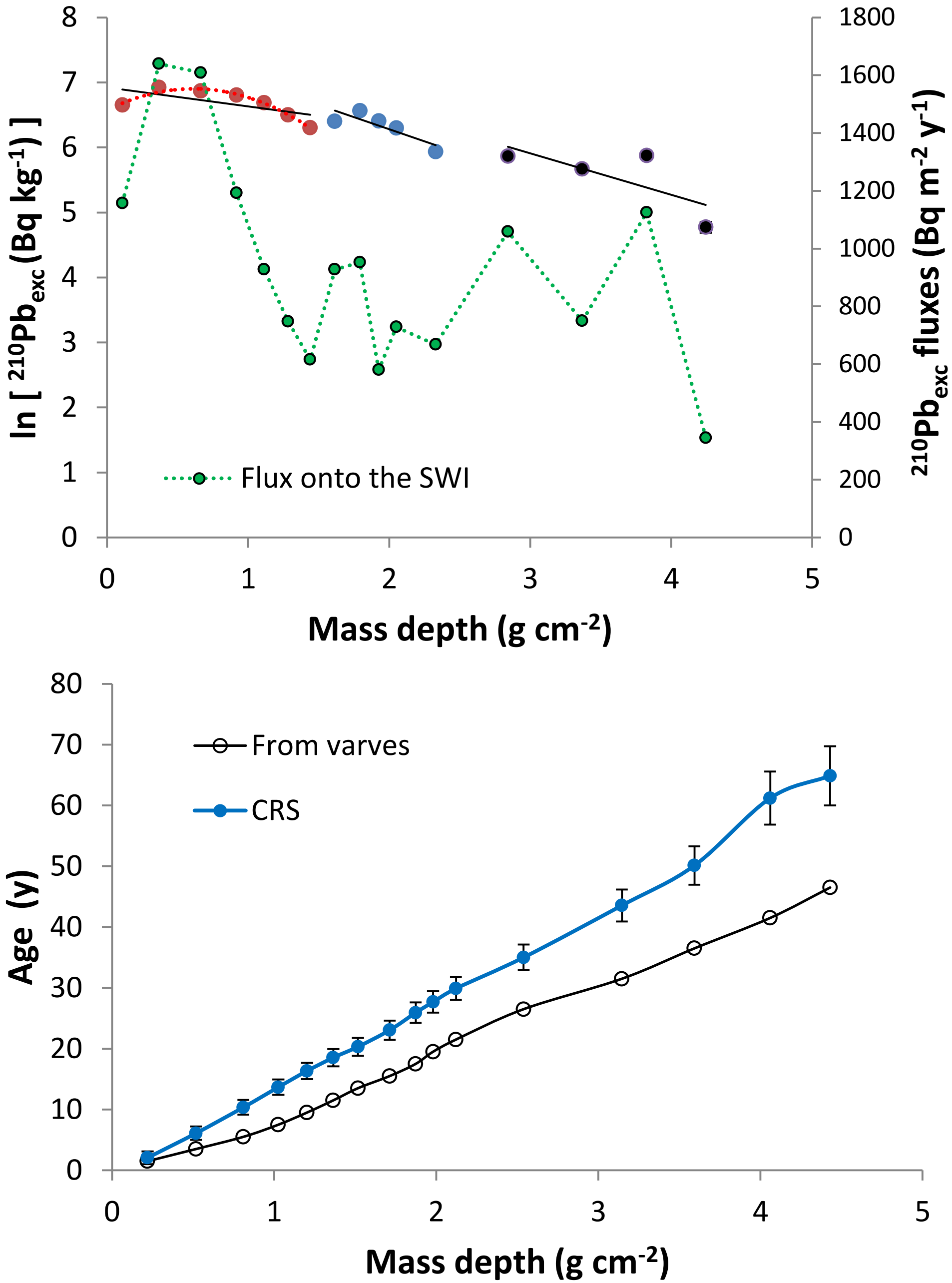

ln [$^{210}Pb_{exc}$ (Bq kg^{-1})]
$^{210}Pb_{exc}$ fluxes (Bq m^{-2} y^{-1})
Flux onto the SWI
Mass depth (g cm^{-2})
Age (y)
From varves
CRS
Mass depth (g cm^{-2})

Fig. 13

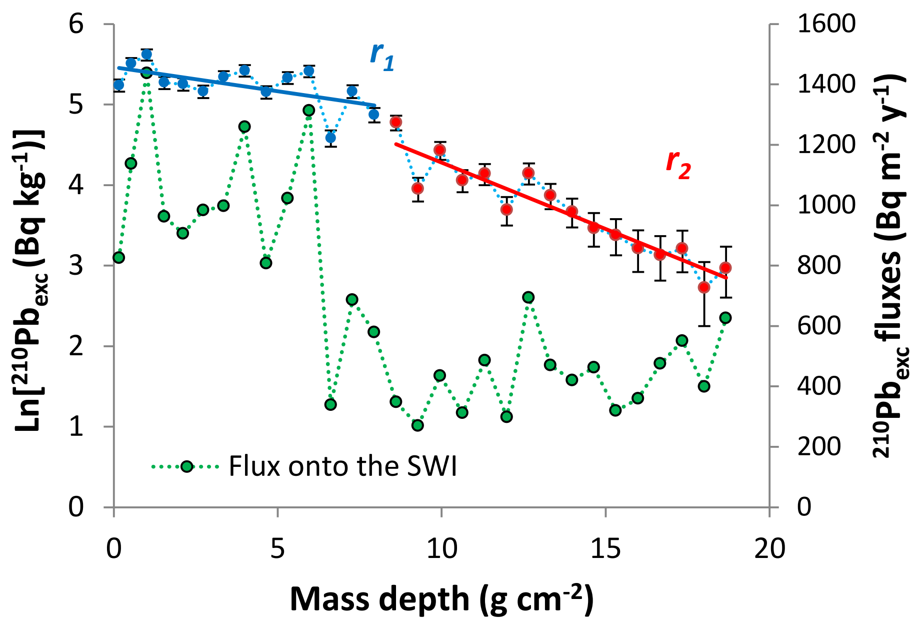

r_1
r_2
Flux onto the SWI
Ln[$^{210}Pb_{exc}$ (Bq kg^{-1})]
$^{210}Pb_{exc}$ fluxes (Bq m^{-2} y^{-1})
Mass depth (g cm^{-2})

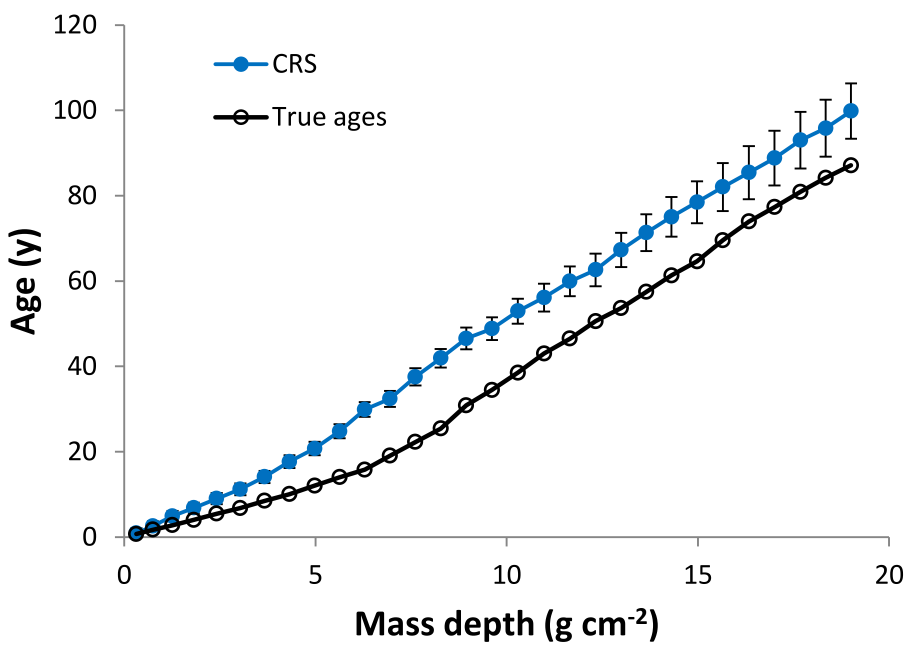

CRS
True ages
Age (y)
Mass depth (g cm^{-2})

Fig. 14

Radiometric dating of recent sediments: On the performance of ^{210}Pb-based CRS chronologies under varying rates of supply

Appendix ESM-A

Theorem: In absence of restrictive assumptions on the variability of fluxes and SARs (the paradigm of the SIT model), any Σ_m versus t_m profile can be translated into an infinite number of different $A(m)$ profiles (and then Σ_m versus m profiles). Inversely, any $A(m)$ profile, without restrictive assumptions else than ideal deposition, continuity of the sequence, and non postdepositional redistribution, can be associated to an infinite number of $\Sigma_m(t_m)$ profiles.

Demonstration: The available data for establishing a ^{210}Pb-based chronology is the $^{210}Pb_{exc}$ versus mass depth profile, $A(m)$. These data allow for the construction of Σ_m vs m profiles (by Eq. 2). The situations for which the CRS model fails (Section 3.4) can be characterised by discontinuities in the slope of the plot Σ_m versus age, as shown in the example of Fig. ESM-A1. As fluxes onto the SWI are related with the initial activity concentration and SAR by its product ($F= A_0\, w$), there is an infinite number of possible combinations of A_0 and w dealing with the same value of F. That is, there is an infinite number of $A(m)$ profiles associated to the same $F(t)$ or $\Sigma_m(t)$ history, each one with its own mass depth scale, and then resulting in different Σ_m vs m profiles, as illustrated in Fig. ESM-A1. In particular, it is always possible to build a mass depth scale (and then a $^{210}Pb_{exc}$ vs m profile) for which Σ_m vs m follows a pure exponential decay ($\Sigma_m = \Sigma_0\, e^{-\beta m}$), namely

$$dm = \frac{1}{\beta} ln\left[\frac{\Sigma(t)}{\Sigma(t+dt)}\right],$$

where β can take a wide range of realistic values.

Consequently, discontinuities in the Σ_m versus age may not be preserved in the Σ_m vs m plot, and some positive cases of warning would not be detected.

On the other hand, for any given $^{210}Pb_{exc}$ vs m profile there are an infinite number of possible chronological lines being mathematically exact solutions (see Fig. 1 and Abril, 2015), and then an infinity number of possibilities for the plot of Σ_m vs t. In particular, there is a chronology for which Σ_m vs t follows an exact exponential, namely the one provided by the raw CRS model.

Although the above arguments apply for discontinuities in the slope of the Σ_m vs m curve, they also hold for any attempt for building an statistical estimator based on $A(m)$.

Figure ESM-A1: Inventory below the sediment horizon at mass depth m (with age t_m), Σ_m, plotted versus age, for fluxes with a stepped variation (Fig. 6a, with parameter values given in the panel). As fluxes relate with SAR and A_0 by their product ($F= A_0\, w$), there is an infinite number of possible $A(m)$ and $\Sigma_m(m)$ profiles sharing the same F(t) history (second panel, with three examples generated for constant w, constant A_0 and random A_0, respectively).

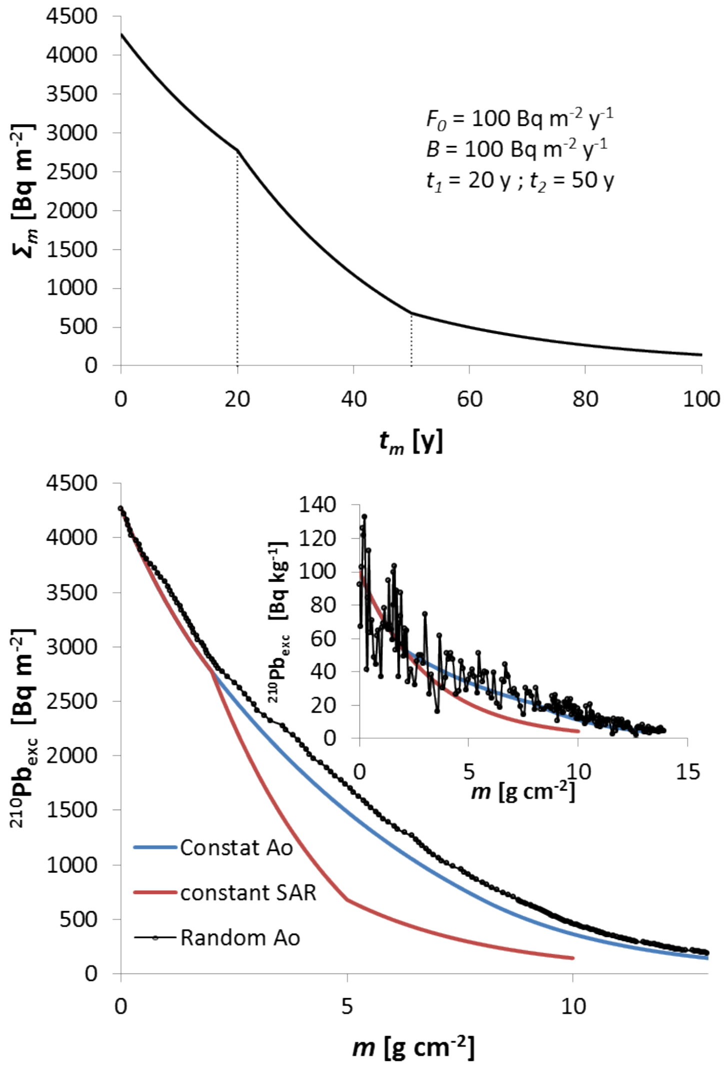

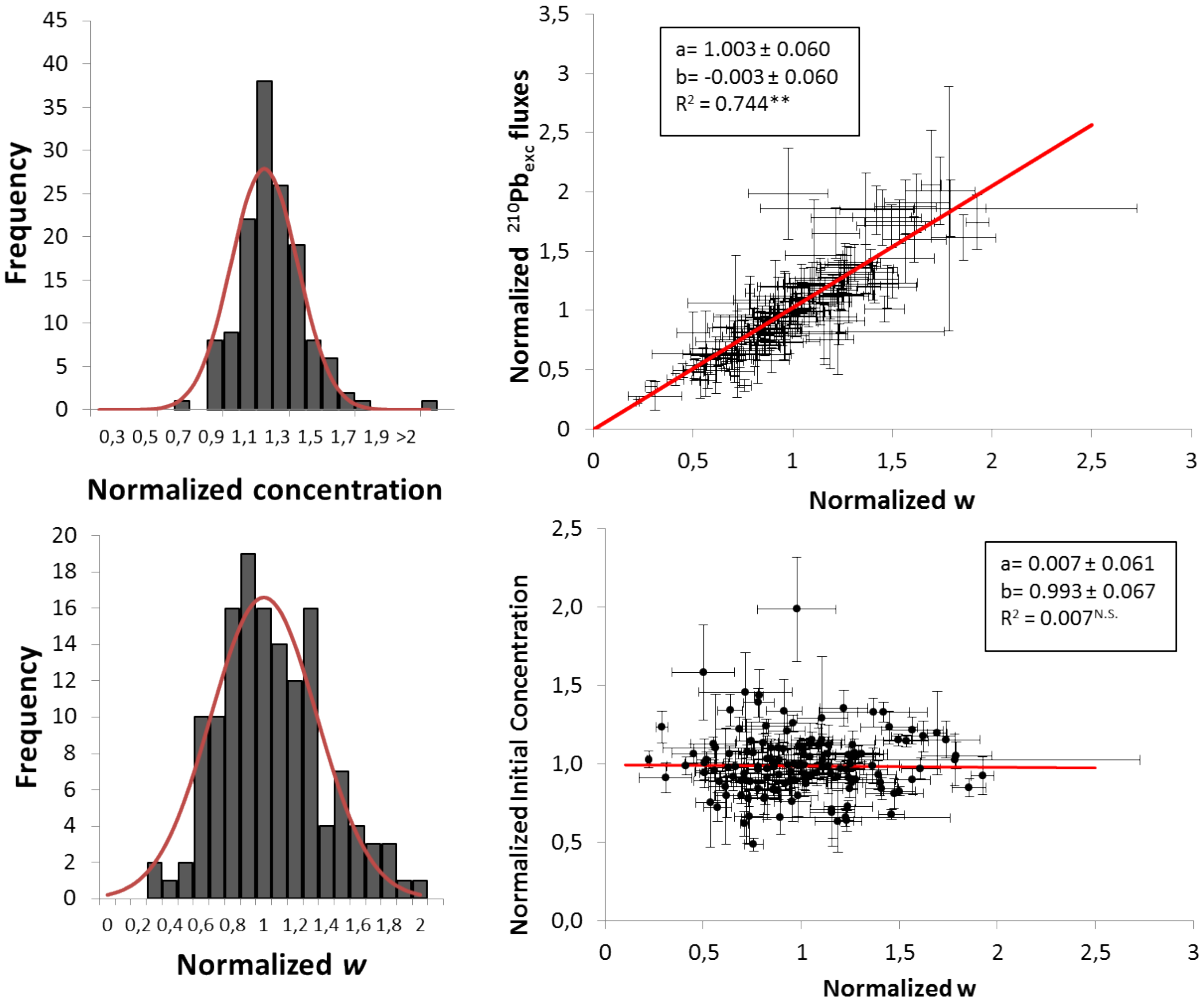

Figure ESM-1 Frequency distributions (left panels) for normalized (to the arithmetic mean of each core) initial activities, and SAR with data from 149 slices from 9 varved sediment cores from marine, riverine a wide diversity of lacustrine environments (Abril and Brunskill, 2014). The continuous line plots the normal distribution for the sake of comparison. Panels on the right show normalized $^{210}Pb_{exc}$ fluxes and initial activity concentrations versus normalized SAR, and linear BCES ((Bivariate Correlated Errors and intrinsic Scatter) regression. Normalization refers to the arithmetic mean value of the magnitude in each sediment core. These statistical features also hold for each single core (Abril and Brunskill, 2014).

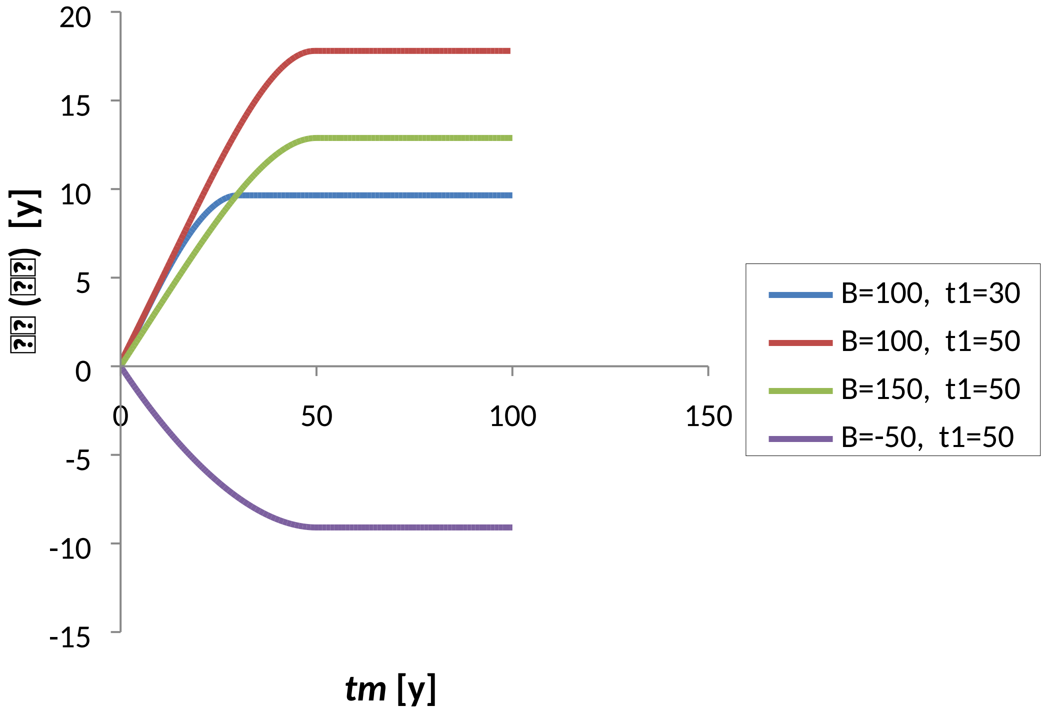

Figure ESM-2. Analytical solutions for the deviation in the CRS chronology under fluxes with a continuous trend of increase/decrease (Fig. 5b). They are depicted for different values of *B* (in Bq·m^{-2}y^{-1}) and t_1 (in years). In all the cases F_0= 100 Bq·m^{-2}y^{-1}. Deviations of the CRS chronology, $\delta_T(t_m)$, have been estimated by Eq. 3, with

$\Sigma_m = \frac{F_0}{\lambda}e^{-\lambda t_1} + \frac{B+F_0}{\lambda}\left(e^{-\lambda t_m} - e^{-\lambda t_1}\right) - \frac{B}{t_1\lambda^2}\left[-\lambda t e^{-\lambda t} - e^{-\lambda t}\right]_{t_m}^{t_1}$ for $t_m < t_1$ and $\Sigma_m = \frac{F_0}{\lambda}e^{-\lambda t_m}$ for $t_m < t_1$.